OPEN ACCESS Freely available online

PLoS one

VAV2 and *VAV3* as Candidate Disease Genes for Spontaneous Glaucoma in Mice and Humans

Keiko Fujikawa[1,3,6]*, Takeshi Iwata[2], Kaoru Inoue[3], Masakazu Akahori[2], Hanako Kadotani[1], Masahiro Fukaya[4], Masahiko Watanabe[4], Qing Chang[5], Edward M. Barnett[5], Wojciech Swat[6]

1 Department of Pathology and Immunology, Hokkaido University Graduate School of Medicine, Sapporo, Japan, **2** National Institute of Sensory Organs, National Hospital Organization Tokyo Medical Center, Tokyo, Japan, **3** Faculty of Health Science, Hokkaido University, Sapporo, Japan, **4** Department of Anatomy, Hokkaido University Graduate School of Medicine, Sapporo, Japan, **5** Department of Ophthalmology and Visual Sciences, Washington University School of Medicine, St. Louis, Missouri, United States of America, **6** Department of Pathology and Immunology, Washington University School of Medicine, St. Louis, Missouri, United States of America

Abstract

Background: Glaucoma is a leading cause of blindness worldwide. Nonetheless, the mechanism of its pathogenesis has not been well-elucidated, particularly at the molecular level, because of insufficient availability of experimental genetic animal models.

Methodology/Principal Findings: Here we demonstrate that deficiency of Vav2 and Vav3, guanine nucleotides exchange factors for Rho guanosine triphosphatases, leads to an ocular phenotype similar to human glaucoma. Vav2/Vav3-deficient mice, and to a lesser degree Vav2-deficient mice, show early onset of iridocorneal angle changes and elevated intraocular pressure, with subsequent selective loss of retinal ganglion cells and optic nerve head cupping, which are the hallmarks of glaucoma. The expression of Vav2 and Vav3 tissues was demonstrated in the iridocorneal angle and retina in both mouse and human eyes. In addition, a genome-wide association study screening glaucoma susceptibility loci using single nucleotide polymorphisms analysis identified *VAV2* and *VAV3* as candidates for associated genes in Japanese open-angle glaucoma patients.

Conclusions/Significance: Vav2/Vav3-deficient mice should serve not only as a useful murine model of spontaneous glaucoma, but may also provide a valuable tool in understanding of the pathogenesis of glaucoma in humans, particularly the determinants of altered aqueous outflow and subsequent elevated intraocular pressure.

Citation: Fujikawa K, Iwata T, Inoue K, Akahori M, Kadotani H, et al. (2010) *VAV2* and *VAV3* as Candidate Disease Genes for Spontaneous Glaucoma in Mice and Humans. PLoS ONE 5(2): e9050. doi:10.1371/journal.pone.0009050

Editor: Patrick Callaerts, Katholieke Universiteit Leuven, Belgium

Received January 22, 2009; **Accepted** January 18, 2010; **Published** February 4, 2010

Funding: The work described in this report was funded in parts by a grant from the Ministry of Education, Culture, Sports, Science and Technology in Japan. The funders had no role in study design, data collection and analysis, decision to publish, or preparation of the manuscript.

Competing Interests: The authors have declared that no competing interests exist.

* E-mail: fujikawa@med.hokudai.ac.jp

Introduction

The critical importance of elevated intraocular pressure (IOP) in the pathogenesis of glaucomatous optic neuropathy is widely recognized [1,2]. While compromise of aqueous humor outflow is the key determinant of elevation in IOP [3,4], the molecular mechanisms underlying changes in the outflow pathway that lead to elevated IOP remain to be elucidated. For this reason, mouse genetic knockout models of spontaneous glaucoma are highly sought after.

The Vav proteins are the best-characterized family of guanine nucleotide exchange factors (GEFs) that activates Rho guanosine triphosphatases (GTPases) in a phosphorylation-dependent manner [5]. Rho GTPases control cell behavior via regulating the specific filamentous actin structures involved in migration, adhesion, and morphogenesis, by acting as binary switches cycling between an inactive (GDP-bound) and active (GTP-bound) state [6]. The three mammalian Vav proteins, Vav1, Vav2, and Vav3, share a Dbl homology domain for their enzymatic activity as GEFs and contain a common structural array characteristic of proteins involved in signal transduction. Regardless of the structural similarity, Vav proteins differ in their tissue distribution. Vav1 is expressed specifically in lymphoid lineage cells, whereas Vav2 and Vav3 are more widely expressed [5,7]. Genetic approaches using knockout mice have provided valuable information on the function of Vav proteins *in vivo*. Vav proteins are crucial for the development and function of hematopoietic lineage cells such as lymphocytes, neutrophils, natural killer cells, and osteoclasts [8–16]. Individual Vav proteins exhibit both redundant and specialized functions. Despite the wide distribution of Vav2 and Vav3 proteins in mouse tissues, little is known about their specific function in non-hematopoietic cells.

While trying to better elucidate the functions of Vav2 and Vav3 in non-hematopoietic cells, we discovered that Vav2/Vav3-deficient mice have a significant ocular phenotype. Specifically, we show that Vav2/Vav3-deficient mice have elevated IOP, which eventually manifests as buphthalmos. Loss of Vav2 and Vav3 expression is associated with changes in the iridocorneal angle, with eventual chronic angle closure. The elevation of IOP in Vav2/Vav3-deficient mice is accompanied by an optic

neuropathy characterized by selective loss of retinal ganglion cells (RGCs) and optic nerve head (ONH) excavation and is therefore consistent with glaucoma. In addition, both *VAV2* and *VAV3* are shown to be susceptibility loci by single nucleotide polymorphisms (SNPs) study of Japanese primary open-angle glaucoma patients.

Results

Vav2/Vav3-Deficient Mice Develop Buphthalmos

Eyes of Vav2/Vav3-deficient ($Vav2^{-/-}Vav3^{-/-}$) mice were noted to develop buphthalmos starting between 6 and 12 weeks of age (Figure 1). This enlargement was typically seen unilaterally at first, with frequent bilateral involvement over the next 1–2 months, and continued enlargement until the mice were 6-months old. Eventually, some of the eyes, became atrophic and phthisical in appearance (Figure 1A). In order to confirm our initial observations, we measured the corneal diameters and weights of $Vav2^{-/-}Vav3^{-/-}$ mice eyes and compared them with age-matched wild-type mice eyes (Figure 1B). The examination clearly showed our observations were relevant. We observed 200 $Vav2^{-/-}Vav3^{-/-}$ mice at 6 months of age and almost 75% of them showed the enlarged eyes (Figure 1C). In addition, histological study indicated that there were no abnormal findings in the tissues both around the enlarged eyes such as inflammation, tumor, or hyperplasia, and in the thyroid of the $Vav2^{-/-}Vav3^{-/-}$ mice (data not shown).

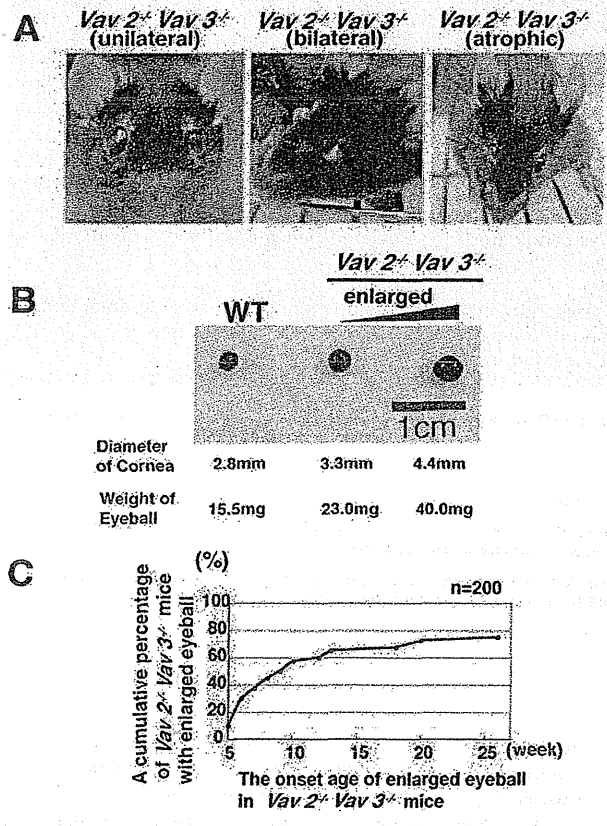

Figure 1. Vav2/Vav3-deficient mice develop buphthalmos. Eyes of Vav2/Vav3-deficient ($Vav2^{-/-}Vav3^{-/-}$) mice develop buphthalmos between 6 and 12 weeks of age. **A.** Left photo: Representative photo of unilateral enlarged eye in 10-week-old $Vav2^{-/-}Vav3^{-/-}$ mice. Centre photo: Representative photo of bilateral enlarged eyes in 16-week-old $Vav2^{-/-}Vav3^{-/-}$ mice. Right photo: Representative photo of enlarged eye becoming atrophic in 8-week-old $Vav2^{-/-}Vav3^{-/-}$ mice. **B.** Comparison of eye sizes. Left panel: Representative eye of 10-week-old wild-type (WT) mice as a control (n = 20). Cornea diameter is 2.9±0.1 mm. Weight is 15.8±1.1 mg. Centre panel: Representative first-recognized enlarged eye of $Vav2^{-/-}Vav3^{-/-}$ mice (9- to 10-week-old, n = 20). The cornea diameter is 3.3±0.1 mm. Weight is 23.7±4.4 mg. $P<0.001$. Right panel: Representative moderately enlarged eye of 12-week-old $Vav2^{-/-}Vav3^{-/-}$mice (n = 20). The cornea diameter is 4.2±0.4 mm. Weight is 38.0±4.0 mg. **C.** Age of onset of enlarged eyes up to 25 weeks of age in $Vav2^{-/-}Vav3^{-/-}$ mice (n = 200). The vertical axis is a cumulative percentage of $Vav2^{-/-}Vav3^{-/-}$ mice with enlargement of the eyes.
doi:10.1371/journal.pone.0009050.g001

Elevation of Intraocular Pressure of Vav-Deficient Mice

As we observed the development of buphthalmos, we assessed for elevated IOP in $Vav2^{-/-}Vav3^{-/-}$, Vav2-deficient ($Vav2^{-/-}$), and Vav3-deficient ($Vav3^{-/-}$) mice. IOP was measured using a rodent tonometer (Tonolab) starting at 4 weeks post-natal and were compared with age-matched wild-type C57BL/6 mice. Reliable measurement of IOP before 4 weeks of age was not possible. At 6 weeks of age, $Vav2^{-/-}Vav3^{-/-}$ mice first showed increased IOP (18.2±3.1 vs. 14.0±2.4 mmHg, $p<0.05$), with further increases out to 10 weeks of age (22.5±7.4 vs. 14.6±4.2 mmHg, $p<0.01$) (Figure 2A). IOP measurements in $Vav2^{-/-}Vav3^{-/-}$ mice ranged from 11–40 mmHg between 7 weeks and 16 weeks of age. There was a statistically significant difference in IOP between the $Vav2^{-/-}Vav3^{-/-}$ and wild-type mice at all time points demonstrated. The phenotype of littermate wild type mice was identical to that of the "inbred" C57BL/6 strain (Figure S1).

In $Vav2^{-/-}$ mice, elevated IOP was first detected at 7 weeks of age. The IOP for $Vav2^{-/-}$ mice was found to be increased at 8 weeks of age compared to wild-type mice (15.5±3.7 vs. 14.0±4.2 mmHg, $p<0.05$)(Figure 2B). The IOP of $Vav2^{-/-}$ mice showed further increases at 10 weeks of age (18.1±3.7 vs. 14.6±4.2 mmHg, $p<0.01$) and remained significantly higher at 12 weeks. In contrast, the IOP of $Vav3^{-/-}$ mice did not differ significantly from wild-type mice between 8 and 12 weeks (Figure 2C). The phenotype of littermate wild type mice was identical to that of inbred strain "C57BL/6". We also demonstrated that the phenotype of Vav2 and Vav3 heterozygous littermate mice ($Vav2^{+/-}$, and $Vav3^{+/-}$) were same as that of wild type (Figure S1).

Retinal Ganglion Cell Loss and Optic Nerve Head Changes in Vav2/Vav3-Deficient Mice

We next examined whether Vav2/Vav3-deficient ($Vav2^{-/-}Vav3^{-/-}$) mice showed changes in the retinal ganglion cell (RGC) layer and optic nerve head (ONH). At 3 weeks of age, $Vav2^{-/-}Vav3^{-/-}$ mice did not show any histological difference in the ONH or the number of RGCs compared to that of age-matched wild-type mice (Figure 3A). At 10 weeks of age, following several weeks of IOP elevation, early signs of ONH cupping and cell body loss in the RGC layer were apparent in $Vav2^{-/-}Vav3^{-/-}$ mice (Figure 3B). At 15 and 30 weeks of age, $Vav2^{-/-}Vav3^{-/-}$ mice showed further evidence of ONH cupping and RGC loss in the context of an otherwise normal retinal architecture. These findings are consistent with a selective loss of RGCs with corresponding changes in the ONH, which are the hallmarks of glaucoma.

Iridocorneal Angle Histopathology in Vav-Deficient Mice

As histopathological examination of globes from mice with buphthalmos frequently demonstrated angle closure, we compared

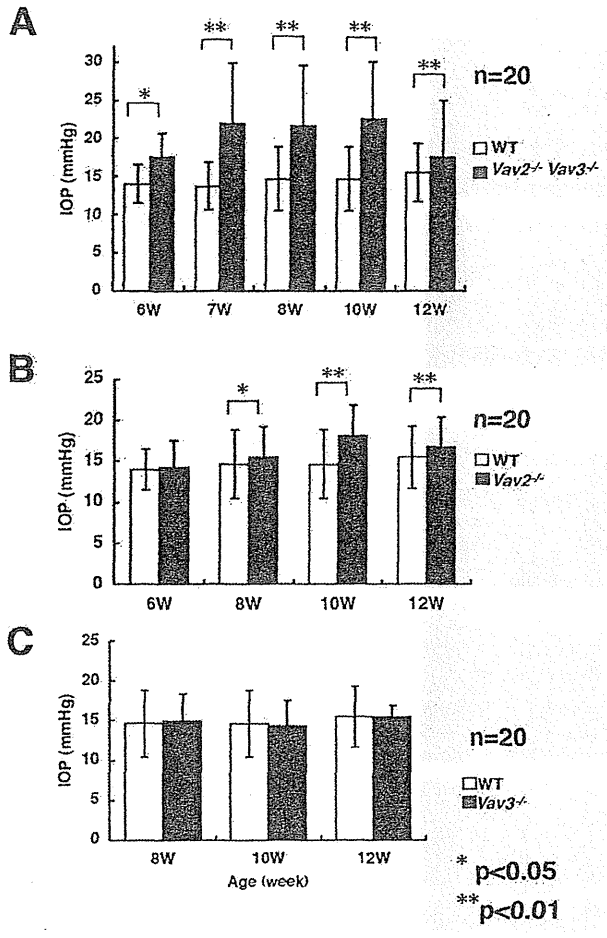

Figure 2. Elevated intraocular pressure of $Vav2^{-/-}Vav3^{-/-}$ and $Vav2^{-/-}$ mice. The intraocular pressure (IOP) of Vav2/Vav3-deficient ($Vav2^{-/-}Vav3^{-/-}$), Vav2-deficient ($Vav2^{-/-}$), and Vav3-deficient ($Vav3^{-/-}$) mice were measured between 10–12 AM. At the indicated ages, twenty mice were examined, respectively. For the IOP measurement of each Vav-deficient mouse, IOP of an age-matched wild-type (WT) mouse was also measured under the same conditions. We confirmed that these results were reproducible with four independent examinations. **A.** IOPs of $Vav2^{-/-}Vav3^{-/-}$ mice were dramatically elevated at 6 weeks of age. **B.** $Vav2^{-/-}$ mice also showed elevated IOP from around 8 weeks of age. **C.** $Vav3^{-/-}$ mice have normal range of IOP at any age. Error bars represent S.D. *P<0.05, **P<0.01 versus WT mice.
doi:10.1371/journal.pone.0009050.g002

the iridocorneal angle histology of 20 Vav2/Vav3-deficient ($Vav2^{-/-}Vav3^{-/-}$) mice with wild-type mice at both 7 and 12 weeks of age. Angles were classified as either being completely open, displaying evidence of partial occlusion of the trabecular meshwork (TM) as manifest by peripheral anterior synechiae (PAS), or being completely closed (total occlusion of the trabecular meshwork)(Figure 4A). Over half of the Vav2/Vav3-deficient mice already showed evidence of angle closure by 7 weeks of age, increasing to nearly 80% in 12-week-old mice (Figure 4B).

We also examined the correlation between elevated IOP and angle changes in 7-week-old $Vav2^{-/-}Vav3^{-/-}$ mice respectively (n = 20) (Figure S2). The mean and standard deviation of IOP in 7-week-old wild-type mice (n = 18) were 13.7±3 12 mmHg respectively. The 95th percentile of those IOPs using a normal curve was 18.8 mmHg. So that IOP over 18.8 mmHg was regarded as elevated IOP. $Vav2^{-/-}Vav3^{-/-}$ mice with elevated IOP showed evidence of angle closure by histological analysis, while $Vav2^{-/-}Vav3^{-/-}$ mice with non-elevated IOP displayed either open angles or evidence of early angle closure (PAS) and angle closure.

In addition, to characterize the progression of angle changes, two additional time points were added to this analysis of the iridocorneal angle −18 days and 4 weeks of age (n = 20 each). While at 18 days of age nearly half of the eyes demonstrated open angles, a large percentage already showed evidence of PAS (Figure 4B). By 4 weeks of age, $Vav2^{-/-}Vav3^{-/-}$ mice showed increasing frequencies of both PAS and angle closure. Taken as a whole, the data showed a gradual progression from open angles to PAS formation to closed angle from 18 days to 12 weeks.

The iridocorneal angles of Vav2-deficient ($Vav2^{-/-}$) and Vav3-deficient ($Vav3^{-/-}$) mice were examined histologically and graded in a similar manner. The iridocorneal angles of $Vav2^{-/-}$ mice also demonstrated evidence of progressive angle closure, but to a lesser extent as compared with $Vav2^{-/-}Vav3^{-/-}$ mice (Figure 4B). $Vav3^{-/-}$ mice had normal appearing open angles without evidence of PAS formation or angle closure (Figure 4B).

In order to better investigate the status of iridocorneal angles in $Vav2^{-/-}Vav3^{-/-}$ mice, we stained for myocilin as a marker for TM cells, as myocilin is strongly expressed in TM cells [17]. We examined 7-week-old $Vav2^{-/-}Vav3^{-/-}$ mice with non-elevated IOP who had either open angles or who displayed evidence of angle closure. As shown in Figure S3, myocilin was not detected in the iridocorneal angle of $Vav2^{-/-}Vav3^{-/-}$ mice with angle closure, but was seen in mice with open angles similar to those of wild-type mice.

Effects of Ocular Hypotensives in Vav2/Vav3 -Deficient Mice

We next tested the efficacy of ocular hypotensives used for human glaucoma in $Vav2^{-/-}Vav3^{-/-}$ mice with elevated IOP (Figure S4). The elevated IOP of 7-week-old $Vav2^{-/-}Vav3^{-/-}$ mice was dramatically reduced by ocular hypotensives used in humans, such as latanoprost, a prostaglandin analogue (Figure S4A). We also tested the IOP-lowering effect in $Vav2^{-/-}Vav3^{-/-}$ mice by two other ocular hypotensives, dorzolamide and timolol, whose mechanisms of action differ from that of latanoprost [18–20], being aqueous suppressants (Figure S4B). Furthermore, we tested Y-27632, a Rho-associated protein kinase inhibitor, that has been reported to cause a reduction in IOP presumably by altering cellular behavior of TM cells [21–23]. Y-27632 showed no effect of lowering IOPs against $Vav2^{-/-}Vav3^{-/-}$ mice, while it lowered the IOP significantly in age-matched wild-type mice (Figure S4C).

Expression of Vav2 and Vav3 in Mouse and Human Eyes

In order to understand the pathogenesis of the Vav2/Vav3-deficient eye phenotype, we examined the mRNA and protein expression patterns of Vav2 and Vav3 in the eye (Figure 5). Quantitative real-time PCR revealed that Vav2 and Vav3 mRNA are expressed in TM, cornea, retina, lens, iris, and ciliary body in the mouse eye (Figure 5A). Vav3 mRNA was more abundantly expressed than that of Vav2 in the TM and the retina. Gene expression levels of both Vav2 and Vav3 in the eye were comparable to levels found in immune cells where Vavs play a critical role [5,7–16]. Next, the Vav2 and Vav3 mRNA localization in mouse eye was examined by in situ hybridization (ISH) analysis (Figure 5B). Both Vav2 and Vav3 oligo probes (antisense), we used here, have been examined the specificities before and proved to have its specificity As negative controls for

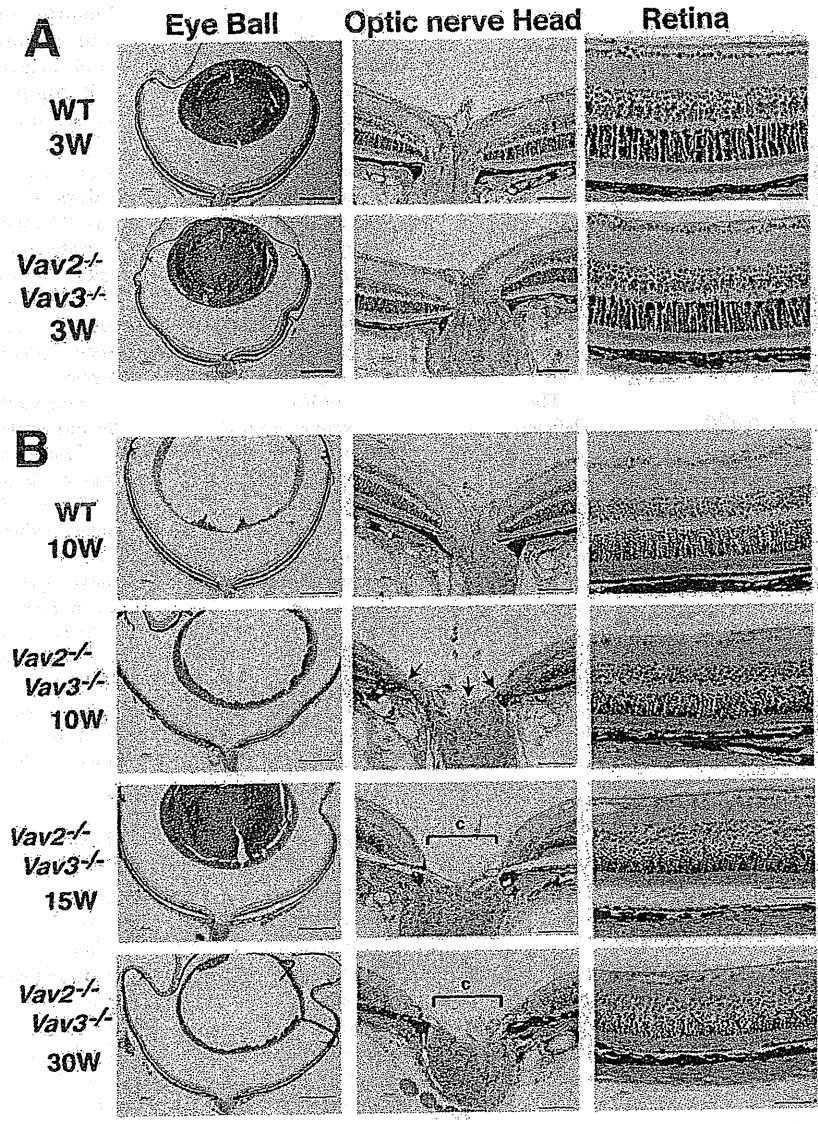

Figure 3. Optic nerve head degeneration and decrease in RGCs observed in *Vav2*$^{-/-}$*Vav3*$^{-/-}$ mice with elevated IOP. Light-microscopic histological examination is conducted to evaluate retinal neuropathy in Vav2/Vav3-deficient (*Vav2*$^{-/-}$*Vav3*$^{-/-}$) mice. **A.** At the age of 3 weeks, *Vav2*$^{-/-}$ *Vav3*$^{-/-}$ mice exhibited impairment of angle status, but no abnormal findings of Optic nerve head degeneration (ONH) or retinal ganglion cells (RGCs) in the retinas. Scale bars, from left to right side: 500 μm, 100 μm, and 50 μm. **B.** After elevation of IOP, compared to control wild-type (WT) mice in the upper panel, ONH in 10-, 15-, and 30-week-old *Vav2*$^{-/-}$*Vav3*$^{-/-}$ mice present so-called capping (shown in c) and thin retinal neural layers (indicated by arrows in the photos). In those retinas, RGCs are decreased. Scale bars, from left to right side: 500 μm, 100 μm, and 50 μm. Sections are representative from 6–12 samples.
doi:10.1371/journal.pone.0009050.g003

these experiments, we used sense probes of Vav2 and Vav3, respectively, which showed no detectable signal (Figure S5). Both genes expression were widely distributed in the ocular tissues including the iridocorneal angle, retina, cornea, and sclera. The co- localization of Vav2 and Vav3 mRNA expression in iridocorneal angle, such as TM, was confirmed by ISH. Also, we assessed Vav2 and Vav3 protein expression by immunoblotting in both mouse and human eyes (Figure 5C). In mouse eyes, expression of both Vav2 and Vav3 was demonstrated in several ocular tissues including the iridocorneal angle, retina, cornea, and sclera. Both Vav2 and Vav3 proteins were also expressed in human retina and iridocorneal angle. The migrated bands were absent in the liver extracts of the *Vav2*$^{-/-}$*Vav3*$^{-/-}$ mice. Results of densitometric ratio (Vav3/Vav2) from normalized protein loading in each lane revealed that Vav3 was more abundantly expressed than Vav2 in the iridocorneal angle tissues of both mouse and human eyes and also in the retina.

Single Nucleotide Polymorphisms in Japanese Primary Open-Angle Glaucoma Patients

We observed Vav2 and Vav3 proteins expression in the tissues of human iridocorneal angle and retina. In order to investigate the

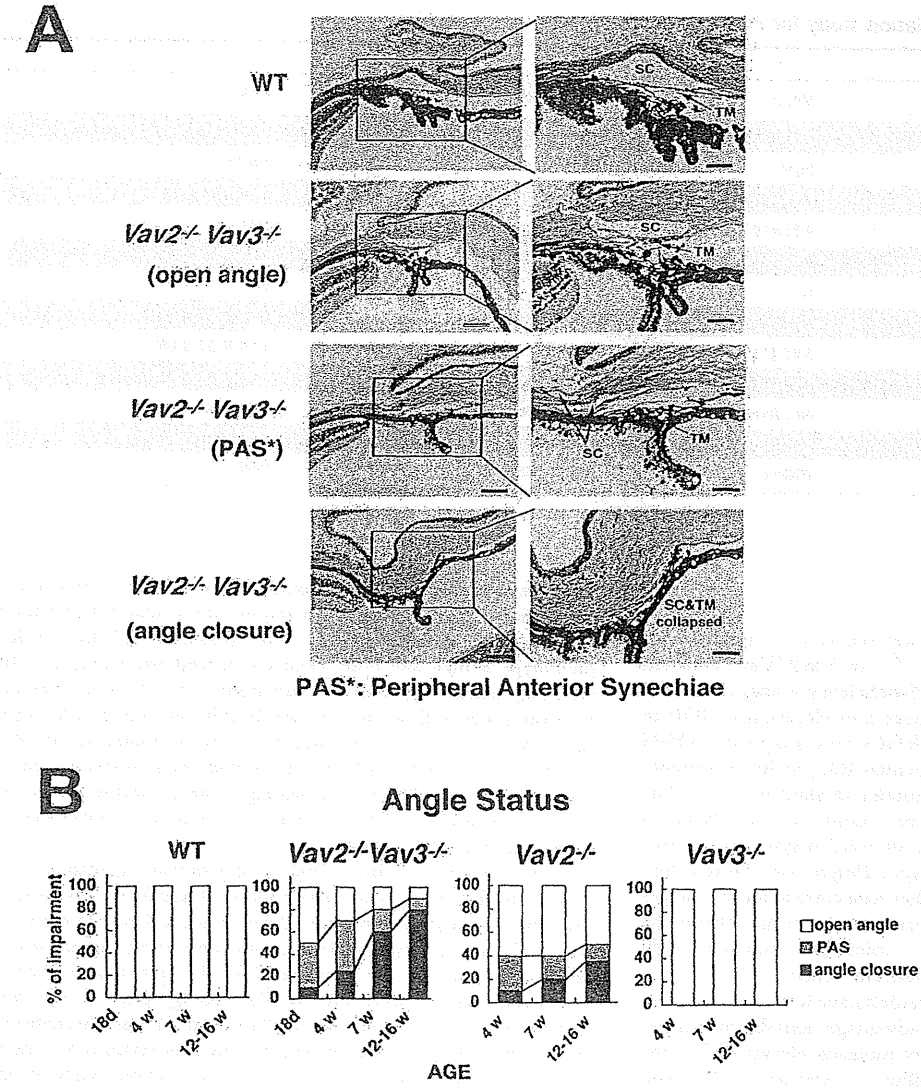

Figure 4. Characterization of progressive iridocorneal angle closures in $Vav2^{-/-}Vav3^{-/-}$ and $Vav2^{-/-}$ mice. The aqueous humor outflow facility, trabecular meshwork (TM) and Schlemm's canal (SC) (iridocornial angle) in Vav2/Vav3-deficient ($Vav2^{-/-}Vav3^{-/-}$) mice are evaluated in histological manner. Vav2-deficient ($Vav2^{-/-}$) mice also have the same changes, but of lower severity. **A.** Representative photos of normal TM and SC histology of 12-week-old wild-type (WT) mice as a control. Representative photos of normal open angle, peripheral anterior synechiae (PAS) in 12-week-old $Vav2^{-/-}Vav3^{-/-}$ mice, and angle closure status in 12-week-old $Vav2^{-/-}Vav3^{-/-}$ mice. Sections used here are all representative from 20 samples. Scale bars: left photos, 200 μm; right photos, 100 μm. **B.** Changes of angle status appear at the early ages. We classify angle status of $Vav2^{-/-}$ $Vav3^{-/-}$, $Vav2^{-/-}$, and $Vav3^{-/-}$mice into open angle, PAS, and angle closure by histological evaluation. We find the changes of angle status at the early ages, such as in 18-day-old $Vav2^{-/-}Vav3^{-/-}$ *mice* (n = 20) and in 4-week-old of $Vav2^{-/-}Vav3^{-/-}$ *mice* (n = 20). We took four ($Vav2^{-/-}Vav3^{-/-}$) and three ($Vav2^{-/-}$, $Vav3^{-/-}$) different age groups, with 20 mice examined, respectively.
doi:10.1371/journal.pone.0009050.g004

relevant association of *VAV2* and *VAV3* in human glaucoma patients, we carried out a genome-wide association study using the Affymetrix GeneChip Human Mapping 500 K Array Set. We examined Japanese primary open–angle glaucoma (POAG) cases and age-matched non-glaucoma controls. Both *VAV2* and *VAV3* loci in Japanese POAG patients showed SNPs against the non-glaucoma controls for dbSNPs rs2156323 and rs2801219, respectively. We reported the most extreme (Table 1). Both were intronic SNPs, SNP rs2156323 lying in intron3 of *VAV2* and SNP rs2801219 lying in intron1 of *VAV3*. *VAV2* SNP rs2156323 in particular indicated significant association with Japanese POAG, including a 5.65 heterozygote odds ratio (95% confidence interval (CI): 1.99–16.0), 4.34 heterozygote relative risk (95% CI: 1.72–10.44) and 4.38×10^{-4} genotypic *P* value with respect to risk allele A.

Judging from allelic *P*-values distribution for detecting *VAV2* ranking and genotypic *P*- values distribution for *VAV3* ranking, we observed that *VAV2* and *VAV3* showed high scores ($-\log_{10}(P)$) among approximately 380,000 SNPs analyzed in this study (Figure 6). On the contrary, *VAV1* showed no association with the POAG. These data strongly suggest that *VAV2* and *VAV3* genes are susceptibility loci in Japanese POAG.

Table 1. Vav2, Vav3, Vav1 association study for POAG using the Affymetrix GeneChip.

Gene	*VAV2*	*VAV3*	*VAV1*
SNP ID	rs2156323	rs2801219	rs2617815
Chromosome Location	9q34.1	1p13.3	19p13.2
Position	133750375	108214454	6746147
Genotypic *P* value	4.38×10^{-4}	5.42×10^{-4}	4.41×10^{-2}
Allele	AG	AC	AG
Risk allele	A	C	G
Minor allele	A	C	G
Heterozygote odds ratio (95%CI)	5.65 (1.99–16.0)	2.03 (1.01–4.09)	1.04 (0.52–2.08)
Heterozygote relative risk (95%CI)	4.34 (1.72–10.44)	1.31 (1.00–1.75)	1.01 (0.82–1.23)
Homozygote odds ratio	Not Available	Not Available	Not Available
Exon Intron	*VAV2* Intron3	*VAV3* Intron1	*VAV1* Intron1
SNP type	iSNP*1	iSNP	iSNP

*1. intronic S.

doi:10.1371/journal.pone.0009050.t001

Discussion

To our knowledge, this is the first report of a spontaneous glaucoma phenotype in Vav2 ($Vav2^{-/-}$) or Vav2/Vav3-deficient ($Vav2^{-/-}Vav3^{-/-}$) mice. Vav2/Vav3-deficiency is associated with progressive iridocorneal angle changes and elevation of IOP in mice. Subsequent selective loss of RGCs and progressive ONH cupping are associated with this elevated IOP, as has previously been demonstrated in other rodent models of glaucoma [24]. The finding that Vav2-deficiency alone results in a glaucoma phenotype suggests that the absence of Vav2 plays a critical role in the development of this phenotype. Despite our finding that Vav3-deficiency did not result in either iridocorneal angle changes or elevated IOP, the more severe glaucomatous phenotype demonstrated in $Vav2^{-/-}Vav3^{-/-}$ mice as compared with $Vav2^{-/-}$ mice is consistent with an additive effect.

A number of induced glaucoma models have been established in rats and mice [24]. Each model has advantages and disadvantages, related to factors such as the ease of inducing elevated IOP, the magnitude, duration and variability of elevated IOP, and secondary effects on the eye. Due to the ease of genetic manipulation, mouse models are becoming increasingly popular over those in rats. Despite the lack of a lamina cribosa as found in human eyes, the mouse is a good genetic model to study the pathogenesis of human glaucoma as aqueous physiology and anterior segment anatomy are similar to that found in humans [25].

Other spontaneous models of glaucoma have been described in mice, most notably in DBA/2J mice. The pigmentary glaucoma phenotype demonstrated in the DBA/2J mice has been extensively studied at genetic, clinical, morphological and pathological levels [26–29]. A limitation of this model is that the elevated IOP phenotype is not primary but secondary due to the systemic pigment dispersion syndrome with the associated mutations in the *Gpnmb* and *Tyrp1* loci [26–30]. In these mice, recessive mutations in these 2 genes are associated with iris degeneration characterized by iris stromal atrophy and pigment dispersion with subsequent reduced outflow facility secondary to pigment and cell debris. Therefore, it is difficult to tie-in the identified mutations to the pathogenesis of any primary form of human glaucoma.

The Vav2/Vav3-deficient mouse has several characteristics which make it particularly useful as an animal glaucoma model. The elevated IOP occurs spontaneously in these genetically manipulated mice and does not require the ocular manipulation necessary in induced models. The frequency of the ocular phenotype is high and onset occurs at a relatively young age. In addition, ocular hypotensives commonly used to treat human glaucoma show efficacy in lowering IOP in this model. The most significant advantage of this mouse glaucoma model is that the deleted genes, Vav2 and Vav3, are well-focused targets that have been studied over 20 years providing a useful starting point for further investigation of the potential molecular mechanisms underlying this phenotype.

Several aspects of this model of spontaneous glaucoma will require further study and clarification, although we speculated from our histological results and the correlation between elevated IOP and angle status changes that anatomic angle closure is the possible mechanism for elevated IOP in this model. While progressive angle closure may be the etiology prior to elevated IOP in mice lacking Vav2 and Vav3 function, it may alternatively be a subsequent change related to other alterations in angle structures which might also affect aqueous humor outflow. In addition, since the expression of Vav2 and Vav3 was detected in ocular tissues other than those comprising the iridocorneal angle, it will be necessary in future studies to consider how their deficiency in these tissues might have potentially contributed to the spontaneous glaucoma phenotype in any way.

While so far there are several reports of glaucoma associated candidate genes based on the single nucleotide polymorphisms (SNPs) study in the Japanese population [31–36], our data first suggest that *VAV2* and *VAV3* are susceptibility loci in Japanese primary open–angle glaucoma (POAG) cases. In addition, so far we could not find the report of non-Japanese glaucoma association case study that demonstrated *VAV2* and/or *VAV3* as candidate gene loci for glaucoma [37–43]. They demonstrated glaucoma associated candidate genes study with SNPs analysis focusing on the other specific target genes, although we are interested in the *VAV2* and/or *VAV3* glaucoma association study using the different populations. This work would be important investigation to be done.

Although our current findings do not address the molecular mechanisms underlying glaucoma phenotypes, it is interesting to consider possible mechanisms based on what is currently known about Vav protein function. The TM has been regarded as a key determinant of IOP and has been implicated as the major site of

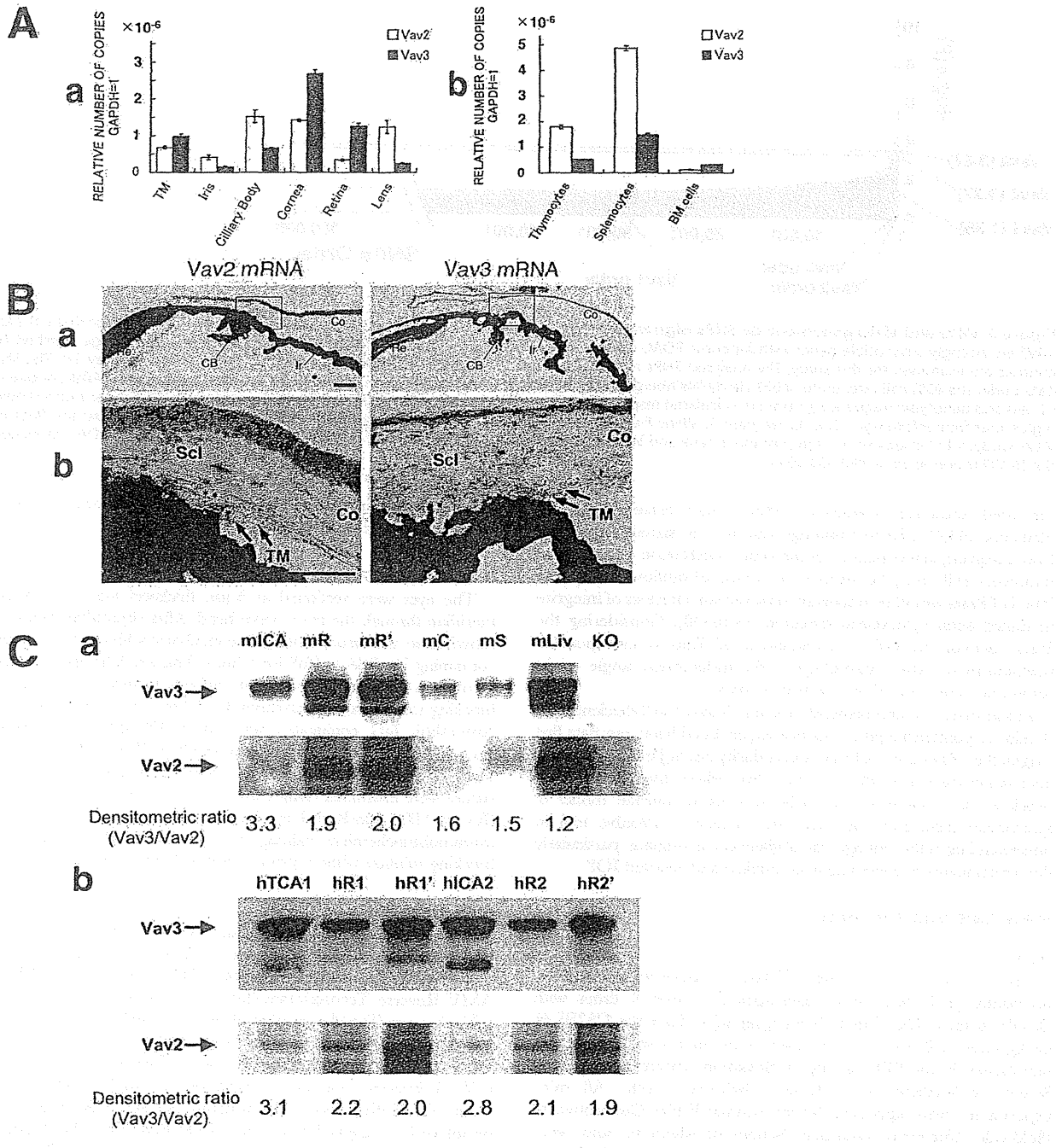

Figure 5. Vav2 and Vav3 expression in mouse and human eyes. A. Quantitative real time PCR analysis is performed for Vav2 and Vav3 mRNA expression study. The vertical axis is the copy number of Vav2 or Vav3 mRNA when that of mGAPDH is taken as 1. The assay method is absolute quantification (standard curve). **a.** Both Vav2 and Vav3 mRNA are expressed in all tissues of the murine eyes including the trabecular meshwork (TM), cornea, sclera, and retina. **b.** Vav2 and Vav3 mRNA expression level of murine immune cells. The levels of Vav2 and Vav3 expression in eye tissues are the same as those of the immune cells where Vav2 and Vav3 play the critical role. **B. a.** In situ hybridization analysis of emulsion-dipped sections display the distribution of Vav2 and Vav3 mRNA in the anterior chamber. The localization of Vav2 and Vav3 mRNA in trabecular meshwork(TM), ciliary body (CB), cornia(CO), iris(Ir), sclera (Scl) and retina(Re) by in situ hybridization. **b.** Vav2 and Vav3 mRNA expression are both detected in iridocorneal angle, such as TM (indicated by arrows in the photos). Scale bars, 50 μm. **C.** Expression of Vav2 and Vav3 proteins in mouse (**a**) and human (**b**) eyes. Vav2 and Vav3 proteins were detected in mouse or human ocular extracts (from two independent postmortem eye globe samples; at death age of 58 (1) and 87 (2)) by western blotting. Densitometric ratios (Vav3/Vav2) were shown under the blotting panels. mICA: mouse iridocorneal angle tissues, mR: mouse retina, mR': 3-fold increased loading mouse retina, mC: mouse cornea, mS: mouse sclera, mLiv: normal mouse liver(positive control), KO: Vav2/Vav3-deficient mouse as a negative control, hICA: human iridocorneal angle tissue,hR1: human retina 1, hR1': human retina1' (3-fold loading).
doi:10.1371/journal.pone.0009050.g005

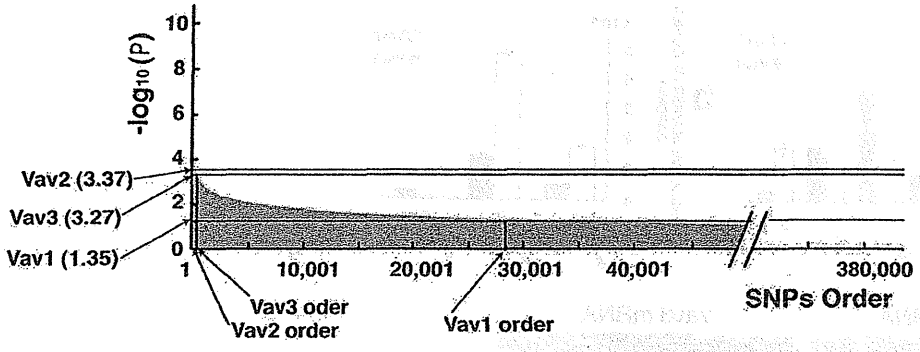

Figure 6. *VAV2* and *VAV3* genome-wide SNPs high ranking of *P*-value scores. Genome-wide ranking orders of *P*-value indicate that *VAV2* and *VAV3* are strongly susceptible genes with Japanese POAG cases. Clinically diagnosed Japanese POAG 100 cases and non-glaucoma age-matched 100 controls are examined for this study. The analysed SNPs number is about 380,000 by the Affymetrix GeneChip 500 K Mapping Array Set. The SNPs data under the 85% call rate, under 0.001 Hardy-Weinberg equilibrium (HWE), and under 5% minor allele frequencies are excluded. Allelic frequency $\chi 2$ test and genotypic frequency $\chi 2$ test are calculated respectively. The vertical axis is −log10 (*P*) and the horizontal axis is SNPs order which showed high scores from left to right. The Upper graph is alleric *P*-values distribution of *VAV2* analysis and the lower graph is genotypic *P*-values for *VAV3* and *VAV1* study. *VAV2* is located at high position in rank and *VAV3* also located at high position in rank. *VAV1* shows no association for POAG cases here.
doi:10.1371/journal.pone.0009050.g006

increased resistance to aqueous outflow which occurs in human glaucoma [44,45]. Recent findings indicate that signals emanating from integrins, key regulators of the actin cytoskeleton in trabecular meshwork cells, may be involved in control of outflow facility and Rho GTPases would be important downstream effectors of integrin-mediated actin cytoskeletal dynamics [4,46–48]. Considering the Vavs function as GEF, dysregulation of Rho is one possible mechanism by which pathology in the iridocorneal angle might result and is one that deserves further study.

In summary, we had demonstrated that Vav2/Vav3-deicient mice develop a spontaneous glaucoma phenotype. In addition, our data first suggest that *VAV2* and *VAV3* are susceptibility loci in Japanese primary open-angle glaucoma (POAG) cases. We believe that Vav2/Vav3-deficient mice will serve not only as a useful murine model of spontaneous glaucoma, but may also provide a valuable tool in understanding of the pathogenesis of glaucoma in humans, particularly the determinants of altered aqueous outflow and elevated IOP.

Materials and Methods

Mice

Vav3$^{-/-}$, *Vav2*$^{-/-}$ and *Vav2*$^{-/-}$*Vav3*$^{-/-}$ mice were described previously [15]. Mice were backcrossed at least 9 times with C57BL/6 mice (Clea Japan, Tokyo, Japan) to have the C57BL/6 background. All mice used in these experiments were bred and maintained in the SPF Facility of Hokkaido University Graduate School of Medicine in a 12-hour light-dark cycle. All mice experiments were approved by the Animal Ethics Committee of Hokkaido University Graduate School of Medicine and were conducted in accordance with the ARVO Statement for the Use of Animals in Ophthalmic and Vision Research.

Tissue Preparation and Histology

Eyes were quickly enucleated from each age group of knock-out mice and C57BL/6 wild-type control mice after deep anesthesia with pentobarbital sodium solution, then immediately fixed with solution of 2.5% glutaraldehyde (TAAB, EM Grade) in 10% formalin neutral buffer-methanol solution deodorized for anterior chamber study, or fixed with Davidson' solution for retinal analysis for 12 hours. Following this, the eyes were embedded in paraffin and dissected sagittally using a microtome into 5 μm sections. After deparaffinization and rehydration, the sections were stained with hematoxylin and eosin (Sigma).

Immunohistochemistry

The eyes were sectioned at 5 μm thickness along the vertical meridian through the optic nerve head. After deparaffinization and rehydration, the tissue sections were incubated with blocking solution containing 1% BSA in PBS for 1 hour. This was followed by 1 hour incubation with rabbit polyclonal antibody to myocilin at 1:200 in blocking solution as first antibody for 1 hour at room temperature. Anti-rabbit IgG conjugated with Alexa 488 (Molecular Probes, Eugene, OR) at 1:400 in PBS containing 0.1% Tween 20 was used as secondary antibody for 1 hour at room temperature. The stained tissues were examined using confocal fluorescence laser microscope (Radius 2000, Bio-Rad, Hercules, CA). For negative control of the immunohistochemical staining, the sections were incubated with blocking solution without primary antibody (data not shown).

Real Time PCR

Each tissue was freshly taken from SPF level C57BL/6 mice and immediately used for generating RNA by TRIzol reagent (Invitrogen). Templates for real time PCR were made by Cloned AMV Reverse Transcriptase (Invitrogen). Probes of mVav2 and mVav3 were TaqMan probes (Vav2: Mm00437287_m1, Vav3: Mm00445082_m1) purchased from Applied Biosystems (Foster city, CA). The standard curves were constructed by mVav2, mVav3 inserted plasmids, normalized by mGAPDH (Product Code: 4352339E, Applied Biosystems). All the PCR studies were performed by Applied Biosystems 7500 Real Time PCR System following the manufacturer's recommended procedures. The assay method was absolute quantification (standard curve).

In Situ Hybridization

The detailed procedure was described as previously [49]. Briefly, to detect mRNAs for Vav2 and Vav3, specific antisense oligonucleotide probes were synthesizedas follows:(2275–2319;45mers)5′-AGCTG-GAGACCGGCTTGAGGCC CTGCTGGTGGTTCGCTCCCG-AGA-3′ for Vav2 mRNA (GenBank accession No. NM_009500) and (2346–2302;45mers)5′–GTTGCCTGTTCTATTACCCCTCTG T CCAGCTGGCTGTTCTGGCTC-3′ for Vav3 mRNA (accession No. NM_020505). Oligonucleotide probes were labeled with [33P]

dATP using terminal deoxyribonucleotidyl transferase (Invitrogen, Carlsbad, CA). Under deep pentobarbital anesthesia, the eyeballs were freshly obtained from Adult C57BL/6J mice. Fresh frozen sections (20 μm thickness) were cut with a cryostat (CM1900, Leica, Nussloch,Germany) and mounted on glass slides precoated with 3-aminopropyltriethoxysilane. Sections were exposed to Nuclear Track emulsion (NTB-2, Kodak) for 5 weeks. Emulsion-dipped sections were stained with methyl green pyronine solution. The specificity of the hybridizing signals was verified by the disappearance of signals when hybridization was carried out with sense probes.

Western Blotting

Mouse Ocular Tissue Dissection: 8-week male C57BL/6J mice (Jackson Laboratory, ME) were used for ocular tissue samples. The animals were euthanized by carbon dioxide inhalation in an induction chamber The globes were promptly enucleated after euthanization and washed in ice-cold PBS. Ocular tissues were microscopically dissected. Dissection of Postmortem Human Eye Globes: Human eyes without previous eye diseases including glaucoma were acquired from a local eye bank (Heartland Lions Eye Banks; Columbia, MO) within 6 hours post-mortem. Dissected mouse and postmortem human ocular tissues were lysed in a tissue extraction buffer (BioChain, CA). The concentration of protein supernatants was determined by a protein assay kit (Bio-Rad, CA). Rabbit polyclonal anti-mouse Vav2 (1:1000) (Santa Cruz Biotechnology, CA), monoclonal anti-human Vav2 (1:2000) (Cell Signaling Technology, MA), polyclonal anti-mouse and anti-human Vav3 (1:3000 for each) (Millipore, CA) antibodies were used for detection.

Intraocular Pressure (IOP) Measurement

IOP was measured using the TonoLab rebound tonometer for rodents (Tiolat i-care, Finland) according to the manufacturer's recommended procedures. All IOP measurements were performed between 10 AM and noon in conscious condition. Mice were gently restrained first by hand and placed on a soft towel bed on the desk and usually appeared calm and comfortable. These data were confirmed to be reproducible by three additional different independent studies ($n \approx 20$).

Evaluation of Eye Drop Medications for High Intra-Ocular Pressure of Vav2Vav3-Deficient Mice

Vav2$^{-/-}$*Vav3*$^{-/-}$ mice were housed in SPF barrier facility in standard lighting conditions (12-hour light-dark cycle). The 7–9 week after birth mice were used for the experiment. Four independent experiments were carried out to confirm the results reproducible.

Preparation and Application of Ophthalmic Solution

Latanoprost was purchased from Cayman Chemical Co. (Ann Arbor, MI) and dissolved in its vehicle solution (0.02% benzalkonium chloride, 0.5% monosodium phosphate monohydrate, 0.6% disodium hydrogen phosphate dihydrate and 0.4% sodium chloride). With a micropipette, 3 μl of PG analogue (latanoprost; prostaglandin F2α) solution or vehicle was randomly applied to the eyes of *Vav2*$^{-/-}$*Vav3*$^{-/-}$ mice. Before administration, IOP was measured with the tonometer from 10–12 AM and then the PG analogue 0.005% 3 μl or vehicle solution was applied in a masked manner. Evaluation of IOP-lowering effect was performed by measuring the IOP with the tonometer at 3 hours after drug instillation also in a masked manner. Furthermore, two different mechanistic medications, 3 μl of timolol maleate (0.5%, Merck, Whitehouse Station, NJ) or 3 μl of dorzolamide hydrochloride (1%, Trusopt; Merck), was also tested, respectively, after measuring the IOP under the same conditions as those of the Latanoprost application. Evaluation of IOP-lowering effects was performed by measuring the IOP with tonometer at 2 hours after drug instillation under blinded test protocols. Y-27632 was purchased from Carbiochem (La Jolla, CA) and dissolved in its vehicle solution (phosphate buffered saline). Y-27632 (1 mM) or vehicle solution was administered to the central cornea as a 3 μl drop by pipetting in a masked manner. Evaluation of IOP-lowering effect was performed by measuring the IOP with the tonometer at 1 hour after drug instillation.

Statistical Analysis of IOPs

Data are reported as means ± S.D. Two-tailed Student's t-test was used to compare between two groups of results. Differences between any two groups were regarded as significant when $P<0.01$(**) or $P<0.05$ (*).

Disease Associated Genome-Wide Analysis

One hundred clinically-diagnosed cases (male 46; female 54) with primary open-angle glaucoma over 30 years of age (mean age, 71.60 years; SD, 9.33 years) and non-glaucoma age-matched controls (mean age, 66.71 years; SD, 12.00 years) in a Japanese population were examined for this study Informed consent was obtained from all participants, and the procedures used conformed to the tenets of the Declaration of Helsinki. Genomic DNAs were isolated from the peripheral blood of the POAG cases and age-matched controls for genotyping analysis. Genotyping was performed using the Affymetrix GeneChip Human Mapping 500 K Array Set (Affymetrix Services Laboratory, California). We omitted the SNP data under an 85% call rate, under 0.001 Hardy-Weinberg equilibrium (HWE), and under 5% minor allele frequency. Data analysis was performed using the LaboServer System (World Fusion, Tokyo Japan). An allelic frequency χ^2 test and genotypic frequency χ^2 test were calculated, respectively with respect to risk allele. The Odds ratio was calculated in three manners such as per allele odds ratio, heterozygote odds ratio, and homozygote odds ratio. Relative risk was also calculated, the same as for the odds ratio. The most significant SNPs were chosen in this report to evaluate the association of *VAV2*, *VAV3*, and *VAV1* in the cases.

Supporting Information

Figure S1 The comparison of intraocular pressures in age matched wild-type inbred C57BL/6 mice, wild-type littermate controls, and Vav2 and Vav3 heterozygous mice (Vav2$^{+/-}$, and Vav3$^{+/-}$). Intraocular pressures (IOPs) were measured using the TonoLab rebound tonometer for rodents from 6-week to 12-week, as described in the Methods. The phenotype of littermate wild-type mice was identical to that of the "inbred" C57BL/6 strain. The phenotype of Vav2 and Vav3 heterozygous mice were similar to that of wild-type. $n = 20$.
Found at: doi:10.1371/journal.pone.0009050.s001 (0.45 MB TIF)

Figure S2 The correlation between elevated IOP and angle changes in Vav2/Vav3-deficient mice. The IOP was measured in 7-week-old Vav2/Vav3-deficient (Vav2$^{-/-}$Vav3$^{-/-}$) mice ($n = 20$), followed by examination of the angle status by histology While Vav2$^{-/-}$Vav3$^{-/-}$ mice with elevated IOP displayed histological evidence of angle closure, mice without elevated IOP showed either normal open angles or evidence of angle changes, angle closure or peripheral anterior synechiae. The mean and standard deviation of IOP in wild-type mice at 7-week-old ($n = 18$) were 13.7±3.12 mmHg, respectively. The 95th percentile of those

IOPs using a normal curve was 18.8 mmHg. IOP over 18.8 mmHg was regarded here as elevated IOP.
Found at: doi:10.1371/journal.pone.0009050.s002 (0.57 MB TIF)

Figure S3 Anti-myocilin staining of trabecular meshwork in Vav2/Vav3-deficient mice. Immunohistochemical staining of trabecular meshwork with anti-myocilin antibody in representative iridocorneal angle sections of age-matched wild-type and Vav2/Vav3-deficient ($Vav2^{-/-}Vav3^{-/-}$) 7-week-old mice with normal IOP, with either evidence of angle closure, or normal open angles similar to wild type mice. Myocilin (green-labeled), which is strongly expressed in TM cells, was regarded as a marker for TM cells. In $Vav2^{-/-}Vav3^{-/-}$ mice with angle closure, myocilin was not detected in the iridocorneal angle (indicated by arrows). Conversely, it was detected in sections from mice with normal open angles, similar to those in wild type mice. Blue fluorescence is DAPI counter staining. Scale bars, 20 um.
Found at: doi:10.1371/journal.pone.0009050.s003 (2.19 MB TIF)

Figure S4 Effects of ocular hypotensives in Vav2/Vav3-deficient mice. A. Ocular hypotensives used for human glaucoma, latanoprost, a prostaglandin analogue was tested in 7-week-old Vav2/Vav3-deficient ($Vav2^{-/-}Vav3^{-/-}$) mice with elevated IOP ($n=20$). The IOP was measured 3 hours before and after topical application of 3 μl of 0.01% latanoprost in a masked manner. Vehicle was used as a control. Latanoprost lowered the IOP significantly in $Vav2^{-/-}Vav3^{-/-}$ mice (26.3 ± 5.0 mmHg versus 15.8 ± 5.1 mmHg; $n=20$), while the IOP was not altered by the vehicle alone. The latanoprost-induced reduction of IOP in $Vav2^{-/-}Vav3^{-/-}$mice was statistically significant (**$P<0.01$, $n=20$). The data shown are representative of three independent experiments performed. Error bars represent S.D. **$P<0.01$ versus vehicle-treated $Vav2^{-/-}Vav3^{-/-}$ mice. B. Using three different drugs for lowering IOP, we compared the effects by percentages of elevated IOP reduction. These data are representative from three independent experiments, respectively ($n=20$). Error bars represent S.D. **$P<0.01$ versus vehicle-treated $Vav2^{-/-}Vav3^{-/-}$ mice. C. Rho-associated protein kinase Inhibitor, Y-27632 was tested for lowering IOP on $Vav2^{-/-}Vav3^{-/-}$ mice ($n=20$). Y27632 administration has no effect against $Vav2^{-/-}Vav3^{-/-}$ mice (before, 19.69 ± 4.98 mmHg; after, 18.83 ± 5.60 mmHg; $n=20$), while Y-27632 lowered the IOP significantly in age-matched wild-type mice (13.58 ± 2.27 mmHg versus 12.31 ± 1.94 mmHg; $n=20$. $p<0.05$) and the IOP was not altered by the vehicle solution (13.25 ± 1.71 mmHg versus 13.18 ± 3.17 mmHg; $n=20$). These data are representative from four independent experiments, respectively. Error bars represent S.D. *$P<0.05$ versus vehicle-treated WT mice.
Found at: doi:10.1371/journal.pone.0009050.s004 (0.41 MB TIF)

Figure S5 Sense probe staining for in situ hybridization experiments in ocular tissues. In situ hybridization with Vav2 and Vav3 sense probes were carried out as negative controls for the experiments. C57BL/6 mouse ocular tissue sections including the iridocorneal angle, sclera and cornea were used. With sense probes, there was no detectable signal around mouse iridocorneal angle tissues. TM; trabecular meshwork. Scl; sclera.
Found at: doi:10.1371/journal.pone.0009050.s005 (4.14 MB TIF)

Acknowledgments

The authors thank Professor Duco Hamasaki (Bascom Palmer Eye Institute, University of Miami School of Medicine, Florida) and Morton Smith, M.D. (Washington University Department of Ophthalmology & Visual Sciences) for helpful suggestions and discussion; and Mr. Tsutomu Osanai and Ms. Takae Oyama for technical help.

Author Contributions

Conceived and designed the experiments: KF TI KI. Performed the experiments: KF TI MA HK MF QC. Analyzed the data: KF TI KI MA MF MW EMB WAS. Contributed reagents/materials/analysis tools: KF TI KI MW WAS. Wrote the paper: KF KI EMB WAS.

References

1. Kass MA, Heuer DK, Higginbotham EJ, Johnson CA, Keltner JL, et al. (2002) The ocular hypertension treatment study: a randomized trial determines that topical ocular hypotensive medication delays or prevents the onset of primary open-angle glaucoma. Arch Ophthalmol 120: 701–713.
2. AGIS investigators (2002) The advanced glaucoma intervention study (AGIS): 7. The relationship between control of intraocular pressure and visual field deterioration. Am J Ophthalmol 130: 429–440.
3. Gabelt BT, Kaufman PL (2005) Changes in aqueous humor dynamics with age and glaucoma. Prog Retin Eye Res 24: 612–637
4. Tan JC, Peters DM, Kaufman PL (2006) Recent developments in understanding the pathophysiology of elevated intraocular pressure. Curr Opin Ophthalmol 17: 168–174.
5. Bustelo XR (2001) Vav protein, adaptors and cell signaling. Oncogene 20: 6372–6381
6. Schmidt A, Hall A (2002) Guanine nucleotide exchange factors for Rho GTPases: turning on the switch. Genes Dev 16: 1587–1609.
7. Turner M, Billadeau DD (2002) VAV proteins as signal integrators for multi-subunit immune-recognition receptors. Nat Rev Immunol 2: 476–486.
8. Swat W, Fujikawa K (2005) The Vav family: at the crossroads of signaling pathways. Immunol Res 32: 259–265.
9. Riteau B, Barber DF, Long EO (2003) Vav1 phosphorylation is induced byβ2 integrin engagement on natural killer cells upstream of actin cytoskeleton and lipid raft reorganization. J Exp Med 198: 469–474.
10. Gakidis MAM, Cullere X, Olson T, Wilsbacher JL, Zhang B, et al. (2004) Vav GEFs are required for β2 integrin-dependent functions of neutrophils. J Cell Biol 166: 273–282.
11. Holsinger LJ, Graef IA, Swat W, Chi T, Bautista DM, et al. (1998) Defects in actin-cap formation in Vav-deficient mice implicate an actin requirement for lymphocyte signal transduction. Curr Biol 8: 563–572.
12. Cella M, Fujikawa K, Tassi I, Kim S, Latinis K, et al. (2004) Differential requirements for Vav proteins in DAP10- and ITAM-mediated NK cell cytotoxicity. J Exp Med 200: 817–823.
13. Doody GM, Bell SE, Vigorito E, Clayton E, McAdam S, et al. (2001) Signal transduction through Vav-2 participates in humoral immune responses and B cell maturation. Nat Immunol 2: 542–547.
14. Faccio R, Teitelbaum SL, Fujikawa K, Chappel J, Zallone A, et al. (2005) Vav3 regulates osteoclast function and bone mass. Nat Med 11: 284–290.
15. Fujikawa K, Miletic AV, Alt FW, Faccio R, Brown T, et al. (2003) Vav1/2/3-null mice define an essential role for Vav family proteins in lymphocyte development and activation but a differential requirement in MAPK signaling in T and B cells. J Exp Med 198: 1595–1608.
16. Tybulewicz VLJ, Ardouin L, Prisco A, Reynolds LF (2003) Vav1: a key signal transducer downstream of the TCR. Immunol Rev 192: 42–52.
17. Karali A, Russell P, Stefani FH, Tamm ER (2000) Localization of myocilin/trabecular meshwork-inducible glucocorticoid response protein in the human eye. Invest Ophthalmol Vis Sci 41: 729–740.
18. Weinreb RN, Toris CB, Gabelt BT, Lindsey JD, Kaufman PL (2002) Effects of prostaglandins on the aqueous humor outflow pathways. Surv Ophthalmol 47 (suppl. 1): S53–S64.
19. Neufeld AH (1979) Experimental studies on the mechanism of action of timolol. Surv Ophthalmol 23: 363–370.
20. Pfeiffer N (1997) Dorzolamide: Development and clinical application of a topical carbonic anhydrase inhibitor. Surv Ophthalmol 42: 137–151.
21. Tanihara H, Inatani M, Honjo M, Tokushige H, Azuma J, et al. (2008) Intraocular pressure-lowering effects and safety of topical administration of a selective ROCK inhibitor, SNJ-1656, in healthy volunteers. Arch Ophthalmol 126: 309–315.
22. Rao PV, Peterson YK, Inoue T, Casey PJ (2008) Effects of pharmacologic inhibition of protein geranylgeranyltransferase type I on aqueous humor outflow through the trabecular meshwork. Invest Ophthalmol Vis Sci 49: 2464–2471
23. Honjo M, Tanihara H, Inatani M, Kido N, Sawamura T, et al. (2001) Effects of Rho-associated protein kinase inhibitor, Y-27632, on intraocular pressure and outflow facility. Invest Ophthalmol Vis Sci 42: 137–144.
24. Pang IH, Clark AF (2007) Rodent models for glaucoma retinopathy and optic neuropathy J Glaucoma 16: 483–505.
25. Aihara M, Lindsey JD, Weinreb RN (2003) Aqueous humor dynamics in mice. Invest Ophthalmol Vis Sci 44: 5168–5173.
26. Chang B, Smith RS, Hawes NL, Anderson MG, Zabaleta A, et al. (1999) Interacting loci cause severe iris atrophy and glaucoma in DBA/2J mice. Nat Genet 21: 405–409.

27. John SW, Smith RS, Savinova OV, Hawes NL, Chang B, et al. (1998) Essential iris atrophy, pigment dispersion, and glaucoma in DBA/2J mice. Invest Ophthalmol Vis Sci 39: 951–962.
28. Goldblum D, Kipfer-Kauer A, Sarra GM, Wolf S, Frueh BE (2007) Distribution of amyloid precursor protein and amyloid-beta immunoreactivity in DBA/2J glaucomatous mouse retinas. Invest Ophthalmol Vis Sci 48: 5085–5090.
29. Schlamp CL, Li Y, Dietz JA, Janssen KT, Nickells RW (2006) Progressive ganglion cells loss and optic nerve degeneration in DBA/2J mice is variable and asymmetric. BMC Neurosci 7 66.
30. Anderson MG, Smith RS, Hawes NL, Zabaleta A, Chang B, et al. (2002) Mutations in genes encoding melanosomal proteins cuase pigmentary glaucoma in DBA/2J mice. Nat Genet 1: 81–85.
31. Nakano M, Ikeda Y, Taniguchi T, Yagi T, Fuwa M, et al. (2009) Three susceptible loci associated with primary open-angle glaucoma identified by genome-wide association study in a Japanese population. Proc Natl Acad Sci U S A 106(31): 12838–12842.
32. Tanito M, Minami M, Akahori M, Kaidzu S, Takai Y, et al. (2008) LOXL1 variants in elderly Japanese patients with exfoliation syndrome/glaucoma, primary open-angle glaucoma, normal tension glaucoma, and cataract. Mol Vis 14: 1898–1905.
33. Shibuya E, Meguro A, Ota M, Kashiwagi K, Mabuchi F, et al. (2008) Association of Toll-like receptor 4 gene polymorphisms with normal tension glaucoma. Invest Ophthalmol Vis Sci 49: 4453–4457
34. Funayama T, Mashima Y, Ohtake Y, Ishikawa K, Fuse N, et al. (2006) SNPs and interaction analyses of noelin 2, myocilin, and optineurin genes in Japanese patients with open-angle glaucoma. Invest Ophthalmol Vis Sci 47: 5368–5375.
35. Inagaki Y, Mashima Y, Fuse N, Funayama T, Ohtake Y, et al. (2006) Polymorphism of b-adrenergic receptors and susceptibility to open-angle glaucoma. Mol Vis 12: 673–680.
36. Ishikawa K, Funayama T, Ohtake Y, Kimura I, Ideta H, et al. (2005) Association between glaucoma and gene polymorphism of endothelin type A receptor Mol Vis 11 431–437
37 Jiao X, Yang Z, Yang X, Chen Y, Tong Z, et al. (2009) Common variants on chromosome 2 and risk of primary open-angle glaucoma in the Afro-Caribbean population of Barbados. Proc Natl Acad Sci U S A 106(40): 17105–17110.
38. Wolf C, Gramer E, Müller-Myhsok B, Pasutto F, Reinthal E, et al. (2009) Evaluation of nine candidate genes in patients with normal tension glaucoma: a case control study. BMC Med Genet 10: 91
39. Narooie-Nejad M, Paylakhi SH, Shojaee S, Fazlali Z, Rezaei Kanavi M, et al. (2009) Loss of function mutations in the gene encoding latent transforming growth factor beta binding protein 2, LTBP2, cause primary congenital glaucoma. Hum Mol Genet 18(20): 3969–3977.
40. Sud A, Del Bono EA, Haines JL, Wiggs JL (2008) Fine mapping of the GLC1K juvenile primary open-angle glaucoma locus and exclusion of candidate genes. Mol Vis 4: 1319–1326.
41 Liu Y, Schmidt S, Qin X, Gibson J, Hutchins K, et al. (2008) Lack of association between LOXL1 variants and primary open-angle glaucoma in three different populations. Invest Ophthalmol Vis Sci 49(8): 3465–3468.
42. Thorleifsson G, Magnusson KP, Sulem P, Walters GB, Gudbjartsson DF, et al. (2007) Common sequence variants in the LOXL1 gene confer susceptibility to exfoliation glaucoma. Science 317(5843): 1397–1400.
43. Kumar A, Basavaraj MG, Gupta SK, Qamar I, Ali AM, et al. (2007) Role of CYP1B1, MYOC, OPTN, and OPTC genes in adult-onset primary open-angle glaucoma: predominance of CYP1B1 mutations in Indian patients. Mol Vis 13: 667–676.
44. Bill A, Svedberg B (1972) Scanning electron microscopic studies of the trabecular meshwork and the canal of Schlemm: an attempt to localize the main resistance to outflow of aqueous humor in man. Acta Ophthalmol 50: 295–320.
45. Wiedelholt M, Bielka S, Schweig F, Lütjen-Drecoll E, Lepple-Wienhues A (1995) Regulation of outflow rate and resistance in the perfused anterior segment of the bovine eye. Exp Eye Res 61· 223–234.
46. Filla MS, Woods A, Kaufman PL, Peters DM (2006) Beta1 and beta3 integrins cooperate to induce syndecan-4-containing cross-linked actin networks in human trabecular meshwork cells. Invest Ophthalmol Vis Sci 47(5): 1956–1967
47 Peterson JA, Sheibani N, David G, Garcia-Pardo A, Peters DM (2005) Heparin II domain of fibronectin uses alpha4beta1 integrin to control focal adhesion and stress fiber formation, independent of syndecan-4. J Biol Chem 25 280(8): 6915–6922.
48. Diskin S, Cao Z, Leffler H, Panjwani N (2009) The role of integrin glycosylation in galectin-8-mediated trabecular meshwork cell adhesion and spreading. Glycobiology 19(1): 29–37
49. Fukaya M, Hayashi Y, Watanabe M (2005) NR2 to NR3B subnit switchover of NMDA receptors in early postnatal motoneurons. Eur J Neurosci 21 1432–1436.

JBC Papers in Press. Published on November 8, 2010 as Manuscript M110.175810
The latest version is at http://www.jbc.org/cgi/doi/10.1074/jbc.M110.175810

PROCESSING OF OPTINEURIN IN NEURONAL CELLS

Xiang Shen[†], Hongyu Ying[†], Ye Qiu[†], Jeong-Seok Park[†], Rajalekshmy Shyam[†], Zai-Long Chi[§], Takeshi Iwata[§], and Beatrice Y.J.T. Yue[†]

From [†]the Department of Ophthalmology and Visual Sciences, University of Illinois at Chicago College of Medicine, Chicago, Illinois, USA and [§]National Institute of Sensory Organs, National Hospital Organization Tokyo Medical Center, Tokyo, Japan

Running head: Processing of Optineurin

Address correspondence to: Beatrice Yue, PhD, Department of Ophthalmology and Visual Sciences, University of Illinois at Chicago, 1855 West Taylor Street, Chicago, IL 60612. Fax: 312-996-7773; E-mail: beatyue@uic.edu

Optineurin is a gene linked to amyotrophic lateral sclerosis, Paget's disease of bone, and glaucoma, a major blinding disease. Mutations such as Glu50Lys (E50K) were identified in glaucoma patients. We investigated herein the involvement of ubiquitin-proteasome pathway (UPP) and autophagy, two major routes for protein clearance, in processing of optineurin in a retinal ganglion cell (RGC) model line RGC5 and neuronal PC12 cells. It was found that the endogenous optineurin level in neuronal cells was increased by treatment of proteasomal inhibitors, but not by autophagic and lysosomal inhibitors. Multiple bands immunoreactive to anti-ubiquitin were seen in the optineurin pull down, indicating that optineurin was ubiquitinated. In cells overexpressing wild type and E50K optineurin, the level of proteasome regulatory β5 subunit (PSMB5, indicative of proteasome activity) was reduced while that for autophagy marker microtubule-associated protein 1 light chain 3 (LC3) was enhanced compared to controls. Autophagosome formation was detected by electron microscopy. The foci formed after optineurin transfection were increased upon treatment of an autophagic inhibitor, but were decreased by treatment of an inducer, rapamycin. The level of optineurin-triggered apoptosis was moreover reduced by rapamycin. The current study thus provides compelling evidence that in normal homeostatic situation, the turnover of endogenous optineurin involves mainly UPP. When optineurin is upregulated or mutated, the UPP function is compromised and autophagy comes into play. A decreased PSMB5 level and an induced autophagy were also demonstrated *in vivo* in RGCs of E50K transgenic mice, validating and making relevant the *in vitro* findings.

Glaucoma is one of the leading causes of irreversible blindness worldwide (1) characterized by progressive loss of retinal ganglion cells (RGCs) and axons, and distinctive cupping of the optic nerve head. The most common form of this disease, primary open angle glaucoma (POAG), is genetically heterogeneous, caused by several susceptibility genes and perhaps also environmental factors (1-4). Currently, a total of 14 chromosomal loci, designated as GLC1A to GLC1N, have been linked to POAG. Three candidate genes identified so far include myocilin (GLC1A), optineurin (GLC1E), and WD40-repeat36 (GLC1G) (1-3). Among them, optineurin is linked principally to normal pressure or normal tension glaucoma (NTG), a subtype of POAG (5). Optineurin mutations were noted to vary with ethnic background (6). The Glu50Lys (E50K) mutation, found in Caucasian and Hispanic populations (6), seems to be associated with a more progressive and severe disease in NTG patients (7). Very recently, optineurin has also been linked to amyotrophic lateral sclerosis (ALS, 8) and Paget's disease of bone (9).

The human optineurin gene codes for a 577-amino acid protein that contains multiple coiled-coil domains and a C-terminal zinc finger (10). The optineurin protein from different species has high amino acid homology (11) and the amino acid 50 glutamic acid residue is conserved in mouse, rat, chicken and cow (12). Optineurin is ubiquitously expressed in non-ocular tissues such as the heart and brain (10) and in ocular tissues including the retina, trabecular meshwork, and non-pigmented ciliary epithelium (9). In the retina, RGCs are immunolabeled with a high intensity (12, 13).

Optineurin shares a 53% amino acid homology with NEMO (NF-κB essential modulator) and was identified as a NEMO-related protein (14). Recently, optineurin has been shown to be a negative regulator of NF-κB (15). Like NEMO, optineurin has a polyubiquitin binding region in the sequence and it binds K-63 linked polyubiquitinated chains (16). Optineurin has in addition been demonstrated to interact with itself to form homo-hexamers (17). It also interacts with proteins including myosin VI, Rab8, and transferrin receptor. Super molecular complexes are detected and granular structures termed foci are formed when optineurin is overexpressed or E50K mutated (17, 18).

Proper processing of cellular proteins is of vital importance. In eukaryotic cells, the ubiquitin-proteasome pathway (UPP) and autophagy are two major routes for protein clearance (19-21). Proteasomes predominantly degrade, in a specific manner, short-lived nuclear and cytosolic proteins. The bulk degradation of long-lived cytoplasmic proteins or organelles is mediated largely by autophagy. Proteins can also be degraded through the autophagy-independent endosome-lysosome system.

Protein degradation via UPP is a temporally controlled and tightly regulated process that involves covalent linking of a single or multiple molecules of ubiquitin to a target protein. The ubiquitinated protein is then marked for degradation by the multi-subunit 26S proteasome complex. The proteolytic core of the complex, the 20S proteasome, contains multiple peptidase activities that include chymotrypsin-like, postglutamyl peptidase or caspase-like and trypsin-like activities. Ubiquitination has been shown to be a pivotal player in regulating a host of cellular processes including cell cycle control, differentiation and quality control (22). It is important not only in cellular homeostasis in tissues/organs including the nervous system but also in degradation of misfolded and aberrant proteins.

Autophagy is an evolutionally conserved mechanism responsible for the nonselective bulk degradation of long-lived proteins and cytoplasmic recycling of organelles during development, tissue homeostasis, and environmental stress such as starvation or amino acid depletion (23, 24). There are three types of autophagy: macroautophagy, chaperone-mediated autophagy, and microautophagy. Among them, macroautophagy (hereafter referred to as autophagy) is the one mediated by the organelle termed autophagosome. Chaperone-mediated autophagy involves the direct translocation of cytosolic proteins across the lysosomal membrane, which requires protein unfolding by chaperone proteins. Microautophagy involves inward invagination of lysosomal membrane, which delivers a small portion of cytoplasm into the lysosomal lumen.

Autophagy begins with the formation of double-membrane bounded autophagosomes (25-27) which then fuse with lysosomes and/or endosomes to form autolysosomes. The contents of autolysosomes are finally degraded by acidic lysosomal hydrolases and the degraded products are transported back to the cytoplasm. Autophagy has been shown to play a role in organelle turnover, cancer cell biology, aging, and neurodegenerative disorders (23, 28-30).

In the present investigation, we determined the involvement of UPP and autophagy in processing of the endogenous optineurin in RGC5 cells, a neuronal cell type recently shown to be of mouse origin (31) and an established model for RGCs (31, 32), as well as neuronal rat adrenal pheochromocytoma PC12 cells (33). The processing of overexpressed wild type optineurin and E50K mutant protein was also studied to test the hypothesis that similar to other neurodegenerative diseases, UPP function is compromised and autophagy is induced with elevated level or mutation of aggregate-prone optineurin.

EXPERIMENTAL PROCEDURES

Cell lines - RGC5 cells were obtained from the University of Illinois at Chicago, Ophthalmology departmental core facility, deposited by Dr. Paul Knepper (34) and originally from Dr. Neeraj Agarwal, North Texas Health Science Center, Fort Worth, TX (31). PC12 cells were purchased from American Type Culture Collection (Masnassas, VA, USA). The cells were cultured in serum-containing complete medium as previously described (18, 35).

In some experiments, RGC5 cells were treated with tumor necrosis factor-α (TNF-α, 100 ng/ml, R & D Systems, Minneapolis, MN) or interferon-γ (IFN-γ, 20 ng/ml, R & D Systems) for 24 h. Both have been shown to elevate the level of optineurin (14, 15, 36). Tetracycline regulated (Tet-on) wild type optineurin ($OPTN_{WT}$)-green fluorescence protein (GFP) inducible stable RGC5 cell line was established as previously described (17). Tet-on inducible E50K optineurin ($OPTN_{E50K}$)-GFP RGC5 cell line was in addition created following the same procedures and strategies. The only exception was that the $OPTN_{WT}$-GFP fragment was replaced with $OPTN_{E50K}$-GFP during the first cloning step (17). The cells were maintained in DMEM complete medium with 10% Tet system certified fetal bovine serum (Clontech, Mountain View, CA), essential and nonessential amino acids, and antibiotics. To induce expression of $OPTN_{WT}$-GFP and $OPTN_{E50K}$-GFP, cells were treated for 16 h with doxycycline (DOX, 1 μg/ml) (Clontech) in DMEM complete medium.

DNA constructs – Optineurin expression vectors pTarget-$OPTN_{WT}$, pTarget-FLAG-$OPTN_{WT}$, pOPTN$_{WT}$-EGFP, pOPTN$_{WT}$-DsRed, as well as pTarget-$OPTN_{E50K}$, pOPTN$_{E50K}$-GFP, and pOPTN$_{E50K}$-DsRed were constructed as previously described (18). Transient transfection was performed using lipofectamine LTX and Plus reagent (Invitrogen,) for 20-48 h according to manufacturer's protocol.

Western blotting - To examine the effects of various inhibitors on levels of the endogenous optineurin, RGC5 and PC12 cells in 6-well plates (300,000 cells/well) were treated for 16 h with vehicle dimethylsulfoxide (DMSO) or H_2O, proteasomal inhibitors lactacystin (LCT, 1 μM) and epoxomicin (5 μM), autophagic inhibitor 3-methyladenine (3-MA, 5 mM), lysosomal inhibitor NH_4Cl (1 mM), or autophagic inducer rapamycin (2 μM). LCT is a proteasomal inhibitor but it also inhibits enzymes such as cathepsin A. Epoxomicin on the other hand is a potent and specific proteasomal inhibitor. 3-MA inhibits class III phosphatidylinositol 3-kinase (PI3K) that is essential for autophagosome formation, as well as other classes of PI3K. It is used as an effective and selective drug to inhibit autophagy degradation. At 5 mM, it has no detectable effects on other proteolytic pathways (27). NH_4Cl is a lysosomotropic weak base that blocks the intralysosomal degradation of macromolecules via inhibition of the acidification of the endosome-lysosome system. It does not affect enzyme activities.

The cells were lysed with lysis buffer (250 mM NaCl, 50 mM Tris/HCl, pH7.5, 5 mM EDTA, 0.5% Nonidet P40) supplemented with protease inhibitor cocktail (Sigma, St. Louis, MO). Protein concentration was determined by bicinchoninic acid protein assay (Pierce, Rockford, IL). Total cell lysate was then subjected to sodium dodecyl sulfate-polyacrylamide gel electrophoresis (SDS-PAGE) under reducing conditions. The proteins were transferred to nitrocellulose membrane and the level of endogenous optineurin was assessed by Western blotting using rabbit anti-C-terminal-optineurin (Cayman Chemical, 1:1000). The membrane was also immunoblotted with polyclonal anti-glyceraldehyde 3-phosphate dehydrogenase (GAPDH, 1:5000, Trevigen, Gaithersburg, MD) for loading control. Immunoreactive protein bands were detected by chemiluminescence using SuperSignal Substrate (Pierce). Densitometry was performed. The band intensity of the endogenous optineurin was normalized to that of GAPDH.

For levels of proteasome regulatory β5 subunit (PSMB5) that is responsible for the chymotrypsin-like activity of the proteasome (37) and an established autophagic marker microtubule-associated protein 1 light chain 3 (LC3) (25), RGC5 and PC12 cells were transfected for 20 h with pTarget empty vector, pTarget-$OPTN_{WT}$ or pTarget-$OPTN_{E50K}$. Total lysate was subject to SDS-PAGE and levels of PSMB5, LC3, and GAPDH were assessed by immunoblotting using polyclonal rabbit anti-PSMB5 (Abcam, Cambridge, MA, 1:1000), monoclonal anti-LC3 (1:1000, Enzo Life Sciences, Farmingdale, NY), and rabbit anti-GAPDH (1:5000).

Immunoprecipitation (IP) - Lysates from RGC5 cells untreated or treated with 1 μM LCT for 16 h were immunoblotted using polyclonal anti-optineurin or monoclonal anti-ubiquitin (1:2000, Biomol, Enzo Life Sciences). Lysates were also immunoprecipitated with rabbit anti-C-terminal-optineurin or rabbit normal IgG (negative control) using the Catch and Release kit (Millipore, Billerica, MA). The proteins pulled down were subjected to SDS-PAGE under reducing

conditions. The ubiquitinated proteins were detected with mouse anti-ubiquitin antibody.

Fluorescence microscopy and immunohistochemistry - RGC5 and PC12 cells were transfected for 20 h with pEGFP-N1 (mock control), pOPTN$_{WT}$-EGFP or pOPTN$_{E50K}$-EGFP. The cells were subsequently treated for 24 or 48 h with autophagic inhibitor 3-MA (5 mM) or overnight with rapamycin (2 μM). The cells were fixed and images were acquired.

For immunofluorescence, the cells were fixed after transfection or treatments, and single or double stained with rabbit anti-optineurin (1:100), rabbit anti-PSMB5 (1:100), or rabbit (MBL International, Woburn, MA) or mouse anti-LC3 (1:100). FITC-goat anti-rabbit IgG, Cy3-goat anti-rabbit IgG, or Cy3-goat anti-mouse IgG (Jackson ImmunoResearch, West Grove, PA; 1:200) was used as the secondary antibody. The slides were mounted in Vectashield (Vector Laboratories, Burlingame, CA) with 4',6-diamidino-2-phenylindole (DAPI).

Photography was carried out using a 63× oil objective on an Axioscope (Carl Zeiss MicroImaging, Thornwood, NY) with the aid of Metamorph software (Molecular Devices, Downingtown, PA). In some experiments, confocal microscopic analysis was performed on a Leica SP2 confocal system (Leica Microsystems, Bannockburn, IL) using the Leica confocal software following sequential scanning to minimize the bleed through.

GFP^u reporter assay – To visualize the change of proteasome activity by optineurin transfection, a GFP^u reporter plasmid (American Type Culture Collection) was used. It is a designer reporter consisting of a short 16-amino acid degron CL1 (a substrate for UPP) fused to the C-terminus of GFP (38, 39). For GFP^u reporter assay, cells co-transfected with GFP^u and pDsRed empty vector (mock control), pOPTN$_{WT}$-DsRed, or pOPTN$_{E50K}$-DsRed for 24 h were examined by confocal microscopy. Images were captured after sequential scanning and the intensity of green fluorescence in at least 60 red-fluorescent transfected cells was quantified.

Transmission electron microscopy: RGC5 cells transfected for 20 h to express GFP, OPTN$_{WT}$-GFP, or OPTN$_{E50K}$-GFP were fixed in 2.5% glutaraldehyde, 2% paraformaldehyde in sodium cacodylate buffer, pH 7.4, postfixed in osmium tetroxide, and embedded in Epon resin. Ultra thin sections (70 nm) were counterstained with uranyl acetate and lead citrate and observed under a JEOL JEM-1220 transmission electron microscope.

For immunogold experiments, inducible cells without or with DOX treatment were fixed at 4°C in 4% paraformaldehyde, 0.1% glutaraldehyde, in phosphate buffered saline, pH 7.4 for 2 h, and sequentially dehydrated in ethanol solutions and embedded in LR-White resin. Sections (90 nm) mounted on 200-mesh nickel grids were blocked and then incubated with polyclonal anti-GFP (1:100, for wild type or E50K optineurin-GFP) and monoclonal anti-LC3 (1:50). The secondary antibodies used were 25-nm colloid gold-conjugated goat anti-rabbit IgG and 10-nm gold conjugated goat anti-mouse IgG (1:25, Jackson ImmunoResearch).

Apoptosis assay - Apoptosis was evaluated by the BIOMOL CV-caspase 3/7 detection kit (Enzo Life Sciences) that utilizes the fluorophore, cresyl violet, coupled to the C-terminus of the optimal tetrapeptide recognition sequences for caspase 3/7, DEVD [CR(DEVD)$_2$]. Cleavage of the target sequences by activated enzymes yields red fluorescence throughout the cell, indicative of apoptotic activity. RGC5 and PC12 cells on glass chamber slides were transiently transfected for 48 h to express GFP, or wild type or E50K optineurin-GFP. Cells were incubated with CR(DEVD)$_2$ for 60 min after treatment with rapamycin for 30 h. The untreated control did not receive rapamycin treatment. The slides were mounted in Vectashield with DAPI which stained nuclei of all transfected and non-transfected cells.

The total number of DAPI-stained transfected cells (green) and the number of CR(DEVD)$_2$-stained transfectants (displaying both green and red fluorescence) in 20 of randomly selected 10x fields were counted (40). The percentage of caspase 3/7-positive apoptotic cells in approximately 100 transfectants (number of green and red cells/number of green only cells) was calculated. The experiments were repeated three times. Statistical analysis was performed using Student's *t* tests.

Transgenic mice - The E50K transgenic mice were generated as previously described (41). All the experiments using mice were performed in

accordance with the Association for Research in Vision and Ophthalmology statement for the Use of Animals in Vision Research.

The IOP of the transgenic mice was measured using an impact-rebound tonometer (Colonal Medical Supply, Franconia, NH) and optical interferometry tonometer (FISO Technologies, Quebec, Canada). Optic disk imaging and light microscopic histopathologic examination of the optic nerve were carried out. Paraffin sections of retinal tissues were prepared for TUNEL assay (39). Sections (5 μm) from 12-month-old normal and transgenic mice were deparaffinized, and stained in parallel with hematoxylin and eosin, monoclonal anti-TUJ1 (anti-βIII-tubulin, 1:400, Covance, Princeton, NJ) to highlight RGC layer (42), or polyclonal anti-optineurin (1:100), anti-PSMB5 (1:250), or anti-LC3 (1:200). Qdot 655 goat anti-mouse or rabbit IgG (1:100, Invitrogen, Carlsbad, CA) was used as the secondary antibody. The slides were mounted in Vectashield, examined under Axioscope, and photographed. In some experiments, sections from 4- and 8-month-old mice were prepared and immunostained with anti-optineurin, anti-PSMB5 and anti-LC3. For EM, 12-month-old mouse eyes were fixed in 2.5% glutaraldehyde, 2% paraformaldehyde in phosphate buffer. The retinas were dissected out and the tissues were postfixed in 1% osmium tetroxide, sequentially dehydrated, and embedded in Spurr's resin. Thin sections (90 nm) were cut and stained for examination under JEOL 1200 EX transmission electron microscope.

RESULTS

Endogenous optineurin level in RGC5 and PC12 cells. Cells were treated with proteasomal, autophagic and lysosomal inhibitors. As can be seen in Fig. 1, the endogenous optineurin level in both RGC5 and PC12 cells was increased by 2-3 fold upon treatment with proteasomal inhibitors, LCT and expoxomicin, but only by 1.1-1.4 fold with autophagic and lysosomal inhibitors. Rapamycin, an autophagic inducer, did not alter the optineurin level, supporting the 3-MA results that autophagy has a minimal role in the processing of the endogenous optineuirn.

Optineurin is ubiquitinated. Lysates from RGC5 cells were immunoprobed for optineurin and ubiquitin. Consistent with results from Fig. 1, the level of optineurin was increased upon treatment of LCT. Also seen were higher molecular weight bands with stronger intensities in LCT-treated samples (Fig. 2A, left panel). Meanwhile, LCT treatment, as anticipated, resulted in an enhanced level of total ubiquitinated proteins in cell lysates (Fig. 2A, right panel).

Lysates were in addition immunoprecipitated with polyclonal anti-optineurin and immunoprobed with monoclonal anti-ubiquitin. Multiple bands immunoreactive to anti-ubiquitin were observed in the immunoprecipitated protein pool, indicating that the endogenous optineurin in RGC5 cells was ubiquitinated (Fig. 2B, left panel). The intensity of the ubiquitin-positive bands was enhanced by prior LCT treatment. The same blot was also probed with anti-optineurin to verify the IP procedure (Fig. 2B, right panel).

Optineurin foci formation. After transfection, the overexpressed optineurin-GFP fusion protein distributed diffusely in the cytoplasm of RGC5 and PC12 cells with dots or granular structures observed most notably near the nucleus (Fig. 3). These structures, referred to as foci, were also observed previously in human retinal pigment epithelial (RPE) and trabecular meshwork cells (18). Foci formation in addition was noted in cells after transfection to overexpress E50K optineurin-GFP. The number and the size of the E50K-GFP foci were greater than those of the wild type (Fig. 3), as was reported previously in RPE cells (18).

Reduced proteasome activity in optineurin overexpressing cells. RGC5 cells transfected for 20 h to express wild type and E50K optineurin-GFP were immunostained for PSMB5 as an indication of proteasome activity (37). The staining intensity in green optineurin-overexpressing RGC5 cells was much reduced compared to mock controls and non-transfected cells (Fig. 4A). Western blot analyses indicated that the PSMB5 protein level was decreased (0.36 ± 0.10 and 0.30 ± 0.14 respectively, $n = 3$, $P < 0.002$) as the optineurin level was increased by 8 to 10 fold upon transfection of pTarget-wild type and E50K optineurin (Fig. 4B). Similar alterations were also observed in PC 12 cells (data not shown).

The cells were subsequently co-transfected with $pOPTN_{WT}$-DsRed and GFP^u reporter plasmid. This ubiquitin proteasome system reporter has been shown to be degraded in mammalian cells in an ubiquitin-dependent manner (38, 39). Proteasomal inhibitors such as LCT, but not other protease inhibitors, increased the steady state level of GFP^u (39). Its fluorescence readout and dependence on ubiquitin thus make GFP^u a simple and reliable tool (30). Results shown in Figs. 4C and D revealed that the GFP^u green fluorescence was increased, indicating a lowered proteasome activity in cells transfected with $pOPTN_{WT}$-DsRed compared to those of DsRed control and non-transfected cells. A decreased proteasome activity was also seen in cells transfected with $pOPTN_{E50K}$-DsRed (Fig. 4C).

Induction of autophagy in optineurin overexpressing cells. Following optineurin transfection, RGC5 (Fig. 5) and PC12 (data not shown) cells were stained for autophagic marker, LC3. The intensity of LC3 staining in optineurin transfected green cells was found stronger than that seen in mock controls and non-transfected cells (Fig. 5A). Partial colocalization between optineurin foci and LC3 staining was observed.

LC3 exists in two forms. LC3-I (18 kDa) is cytosolic and LC3-II (16 kDa) is lipidated (conjugated to phosphatidylethanolamine) that inserts into the membrane. The amount of LC3-II is correlated with the extent of autophagosome formation and increasing levels of LC3-II on immunoblots have been used to document induction of autophagy (27). In RGC5 cells, the level of LC3 protein, especially the active LC3-II form, was found substantially increased (2.4 ± 0.4 and 2.7 ± 0.5 respectively, $n = 5$, $P < 0.002$) by Western blotting upon overexpression of wild type and E50K optineurin (Fig. 5B).

In separate experiments, RGC5 cells were treated with TNF-α and IFN-γ for 24 h. The optineurin level was increased by approximately 2 fold, as was reported previously (14, 15, 36). Foci formation was not apparent but the PSMB5 level was found reduced by 40 to 60% while the LC3-II level was elevated by 1.9 to 2.5 fold (Fig. 6). Similar PSMB5 and LC3 alterations were also observed in inducible cell lines when wild type and E50K optineurin-GFP levels were induced by 10-12 fold and foci were formed upon DOX treatment (data not shown). It is of note that the overexpressed or upregulated optineurin levels seen in Figs 4-6 are not the expression levels, but rather the stationary state levels set by expression and degradation. The resulting level depends not only on the translational increase, but also on the maximum ability of the cell to degrade the excess proteins. This indicates that the transient overexpression might be much higher than 10X, but could be regulated somewhat by the autophagic degradation process.

Furthermore, electron dense as well as electron-light double- or multiple-membrane autophagosome- and autolysosome-like structures or vesicles (43, 44) were prominently observed by electron microscopy in RGC5 cells after optineurin transfection (Fig. 7A, a-c). These structures were rarely detected in GFP control (Fig. 7Ad) and non-transfected (data not shown) cells.

Autophagosome-like structures were also observed in inducible wild type (data not shown)- and E50K (Fig. 7B, a and b)-GFP-expressing cells following DOX induction, but not in non-induced cells (Fig. 7Bb, insert). Immunogold studies showed co-localization of E50K optineurin-GFP and LC3 in autophagosome-like structures (Fig. 7B, c and d).

Optineurin foci formation is regulated by autophagy. RGC5 (Fig. 8, A and B) and PC12 (data not shown) cells transfected with $pOPTN_{WT}$-GFP and/or $pOPTN_{E50K}$-GFP for 20 h were treated with 3-MA or rapamycin for 24 or 48 h. The 3-MA treated cells showed more optineurin wild type foci formation compared with the untreated controls (Fig. 8A) and the foci enhancement was more dramatically seen at the 48-h time point. The rapamycin treated cells on the other hand, showed less foci formation compared with untreated group in both $pOPTN_{WT}$-GFP- and $pOPTN_{E50K}$-GFP-transfectants (Fig. 8B), suggesting that the overexpressed optineurin was cleared, at least in part, via the autophagy pathway.

Rapamycin treatment reduces the level of apoptosis induced by overexpressed optineurin. RGC5 (Fig. 8C) and PC12 (data not shown) cells were transiently transfected to express GFP alone, wild type or E50K optineurin-GFP followed by treatment of rapamycin. Images were captured and the percentage of cells that exhibited activated caspase 3/7 enzymes, representing apoptotic activity, in the transfected population was determined. Results indicated that without the

rapamycin treatment, the percentage of caspase 3/7-positive cells in total wild type and E50K optineurin-GFP-overexpressing transfectants was increased by approximately 1.8 to 2.5 fold ($P < 0.008$) compared to that in pEGFP-N1-transfected mock controls (Fig. 8C). After the rapamycin treatment, the level of apoptosis in optineurin transfectants was declined to within the control limits (Fig. 8C).

Transgenic E50K mouse. The E50K mouse is transgenic, not a knock-in mouse. The transgene was expressed using the chicken β-actin promoter (pCAGGS) with CMV enhancer. The copy number for the mutant gene was approximately 12 to 14 per mouse (41). While the distribution remained similar, the overall optineurin expression was higher in the retina of E50K transgenic mice compared with the endogenous optineurin expression. The RGC loss and retinal thinning were seen 12 month after birth in the transgenic mice. By 16 months, approximately 43% of the retinal thickness and approximately 20% of RGC numbers were reduced (41). Excavation of the optic nerve head was also observed. Apoptotic RGCs were detected in 16 month or older E50K mice. The average IOP reading for mutant mice was in the normal range of 15 ± 1 mmHg for all examined ages (41).

Tissue sections from 12-month-old E50K transgenic mice displayed a fainter staining of PMSB5 but a stronger staining of LC3 in RGCs compared with those from control littermate mice (Fig. 9B). Staining with anti-optineurin also yielded a higher intensity in the transgenic tissues as expected (Fig. 9B). The enhanced LC3 and reduced PSMB5 staining was also observed in sections from the 4- and 8-month-old transgenic mice (data not shown). Interestingly, no pathology was apparent in the former mice while retinal thickness appeared to be somewhat reduced in the latter.

The staining results in 12-month-old E50K transgenic and normal mice were confirmed by Western blotting of retinal extracts (Fig. 9C). By electron microscopy, autophagosome-like structures were demonstrated in RGCs of E50K transgenic eyes (Fig. 9D). Quantification analyses indicated that the structures were found in 22 of 33 RGCs examined in transgenic mouse sections, but only in 1 of 23 RGCs in controls.

DISCUSSION

In eukaryotic cells, the ubiquitin-proteasome and autophagy pathways are two major routes for protein clearance (19-21). The present study demonstrates that proteasomal inhibition led to an increase in the endogenous optineurin level in neuronal RGC5 and PC12 cells (Fig. 1). On the other hand, autophagic and lysosomal inhibition as well as autophagic activation had little effects. The UPP thus appeared to be the major pathway for endogenous optineurin processing. Autophagy and lysosomes had a rather minor, if any, role. Supporting this conclusion, the endogenous optineurin in RGC5 cells was found ubiquitinated (Fig. 2). UPP has been shown to be the pathway that degrades in a specific manner short-lived proteins. The involvement of UPP is therefore consistent with our finding that the half life of the endogenous optineurin is approximately 8 h (17). Ubiquitination of the endogenous optineurin also agrees with a previous observation that ^{35}S-labeled, *in vitro*-translated optineurin binds to ubiquitin and is ubiquintinated (16).

Our study further indicates that upon optineurin overexpression or mutation, the proteasome activity in neuronal cells is decreased (Fig. 4) while autophagy is induced. The induction of autophagy is evidenced by an increased immunostaining (Fig. 5A) for an established autophagic marker LC3 (25), an increased protein level of LC3-II (Fig. 5B), the lipidated form of LC3 that inserts into the membrane and correlates with the appearance of LC3-positive autophagosomes (27, 45-47), plus the detection of autophagosome- and autolysosome-like structures in transfected cells (Fig. 6). The overexpressed wild type and E50K optineurins appeared to be processed largely through autophagy, as autophagic activator rapamycin diminishes, while the inhibitor 3-MA augments the foci formation (Fig. 8, A and B).

A decrease in the PSMB5 level and an increase in the LC3 level were similarly observed in cells treated with TNF-α and IFN-γ (Fig. 6) as well as in inducible cell lines (data not shown). Such *in vitro* changes were likewise observed *in vivo* in E50K transgenic mice. The E50K-overexpressing mice developed phenotype that mimicked the clinical features of NTG patients including neuropathy of the optic disc and

degeneration of the RGCs without an increased IOP (41). This mouse line thus appears to be the first NTG mouse model. It is notable that the intensity changes of PSMB5 and LC3 staining, although not dramatic, were readily visible (Fig. 9B). The protein level changes in the 12-month-old E50K mice were confirmed by Western blotting (Fig. 9C). Autophagosome- and autolysosome-like structures were also observed in the E50K specimens (Fig. 9D).

It has been documented that when a cytosolic protein is aggregate-prone, it becomes a poor proteasome substrate. One example is α-synuclein, a protein of unknown function and a major component of Lewy bodies (aggregates) observed in Parkinson's diesease. Mutations of α-synuclein are known to cause autosomal dominant, early-onset Parkinson's disease. Previous studies have disclosed that both UPP and autophagy are routes for α-synuclein degradation and that while soluble α-synuclein is cleared by proteasome, the aggregated protein or mutants are preferentially cleared by autophagy (30, 47).

The optineurin degradation hence parallels that described for α-synuclein. The endogenous optineurin seems to be degraded chiefly through the ubiquitin pathway. When optineurin is upregulated or mutated in neuronal cells, autophagy becomes involved (Figs. 5-7).

The optineurin overexpression characteristics bear similarities to those seen in neurodegenerative diseases including Alzheimer's and Huntington's (20, 48, 49). After transfection with wild type or E50K optineurin, the optineurin foci are observed to distribute in perinuclear region in proximity to the Golgi complex (17, 18, 40). Following precedent of those described for aggresomes, inclusion bodies or Lewy bodies, the optineurin foci are formed in a microtubule-dependent manner (17, 18). They appear to be LC3-positive (Fig. 5A). Also, the proteasome function is impaired (Fig. 4, C and D) as was seen in neurodegenerative diseases (49-51). In addition, overexpression of both wild type and E50K optineurin leads to apoptosis in cultured cells (40) and the toxicity can be rescued by rapamycin treatment (Fig. 8C). These analogies further underline that glaucoma shares common features with neurodegenerative diseases (52-54).

The role or significance of the foci observed in glaucoma is at present unclear. Interestingly, the roles of inclusion bodies and aggresomes formed in other neurodegenerative diseases are also not clear. As summarized in a number of reviews (21, 26, 55, 56), the inclusion bodies and aggresomes may play protective role by sequestering toxic, misfolded protein species and providing the cells with an opportunity of delayed protein degradation. They may also inactivate the proteasome and mediate cytotoxicity. Inhibition of proteasome is believed to induce autophagy, which serves as a default mechanism for degradation of the accumulated abnormal proteins. However, when the autophagic clearance system reaches saturation, unable to eliminate the excess proteins, dysregulation or defection may occur, contributing to apoptosis and pathology (26). Supporting this notion, diffuse and abnormal proteins accumulate and aggregate to form inclusions which can disrupt the neural system in Atg5 (autophagy-related gene 5) deficient mice (57). Also, the protein accumulation and neurodegenerative phenotype could be reverted by activation of the autophagy pathway with a gene therapy approach (58) or infusion of rapamycin (55). It is suggested that there may exist a threshold as a point of divergence between physiological and pathological autophagy (59) and both the physiological and pathological roles of autophagy remain as critically important areas for investigations. Furthermore, inhibition of proteasome function has also been shown to trigger apoptosis (60) depending on cell types and conditions. Defects in the UPP may drive human pathologies including neurodegenerative diseases (30) although there have been controversies that still await further clarification (61).

A similar scenario may take place in optineurin-related glaucoma. In this context, it is intriguing that a persistent accumulation of autophagosomes was observed in a recent study (62) in the rat optic nerve following an optic nerve crush injury. The autophagy observed, possibly related to the lesion-induced calcium influx, was thought to be the major pathophysiological mechanism contributing to the ensuing axonal degeneration. It is also of interest that very recently mutations of optineurin are reported to be involved in the pathogenesis of ALS (8). While the role of foci in pathology remains to be precisely defined, an ALS case with the E478G optineurin mutation did show optineurin- and

ubiquitin-positive cytoplasmic inclusions. Optineurin in addition is linked to Paget's disease (9), a condition characterized by focal increases in bone turnover. The osteoclasts in affected bone also contain intranuclear inclusion bodies (63).

There is growing evidence that ubiquitin may be involved in "selective" autophagy (21, 64). It has been shown that ubiquitin binding receptors such as p62 are required in the process of autophagic clearance of protein aggregates (61, 64). By binding simultaneouly to ubiquitin and autophagosome-associated ubiquitin-like LC3, the receptors mediate docking of ubiquitinated protein aggregates to the autophagosome for selective degradation. Optineurin is ubiquitinated, whether its aggregates are processed through the "selective" autophagy process is currently unknown.

Taken together, the current study provides compelling evidence that in normal homeostatic situation, the turnover of endogenous optineurin involves mainly UPP. When optineurin is upregulated or mutated, the UPP function is compromised and autophagy comes into play. A decreased PSMB5 level and an induced autophagy were also demonstrated *in vivo* in RGCs of E50K transgenic mice, validating and making relevant the *in vitro* findings.

Optineurin and E50K mutant have been shown to inhibit NF-κB activation (8, 15). Studies from our laboratory reveal that the interaction with Rab8 and transferrin receptor is stronger with E50K mutant than the wild type optineurin. The mutant also produces a more prominent foci formation (17, 18), more severe fragmentation of the Golgi complex (18), and a higher level of apoptosis (40) than overexpression of the wild type optineurin. Representing a gain-of-function mutation, E50K in addition impairs more dramatically the transferrin trafficking (65). Based on these observations, we surmise that the defective trafficking, deregulated NF-κB signaling, along with fragmentation of the Golgi complex and increased apoptosis may be the underlying bases how E50K optineurin mutation renders the patients predisposed to the glaucoma pathology. Autophagy, on the other hand, may not be a primary factor in the disease development. This pathway may simply be induced initially as a protective response with build-up of the aggregate-prone mutant protein. Autophagy may contribute to the demise of the cells only when the build-up exceeds the capacity, exacerbating then the disease condition.

It is additionally noteworthy that while the E50K findings have pathologic significance, the wild type optineurin overexpression results may also be of physiologic relevance. Optineurin, for example, is known to be upregulated by proinflammatory cytokines TNF-α (14, 36) and IFN (14). Its expression may be heightened to set off adverse consequences upon acute or chronic inflammation and infection. Increases of TNF-α in the retina and the optic nerve head have been associated with glaucomatous conditions (66).

Knowledge of the degradation pathways acting on optineurin can help in design of novel therapeutic strategies (30). For example, proteasome activity can be promoted by overexpression of proteasome subunit or molecular chaperones and autophagy can be upregulated by rapamycin (30), rapamycin plus lithium combination (67), or small molecule autophagy enhancers (68). Future studies will be focused on this translational aspect.

REFERENCES

1. Allingham, R. R., Liu, Y., and Rhee, D. J. (2009) *Exp. Eye Res.* **88**, 837-844
2. Wiggs, J. L. (2007) *Arch. Ophthalmol.* **125**, 30-37
3. Kwon, Y. H., Fingert, J. H., Kuehn, M. H., and Alward, W. L. M. (2009) *N. Engl. J. Med.* **360**, 1113-1124
4. Wang, N., Chintala, S. K., Fini, M. E., and Schuman, J. S. (2001) *Nat. Med.* 7, 304-309
5. Rezaie, T., Child, A., Hitchings, R., Brice, G., Miller, L., Coca-Prados, M., Heon, E., Krupin, T., Ritch, R., Kreutzer, D., Crick, R. P., and Sarfarazi, M. (2002) *Science* **295**, 1077-1079